Univerzita Karlova v Praze

Matematicko-fyzikální fakulta

DIPLOMOVÁ PRÁCE

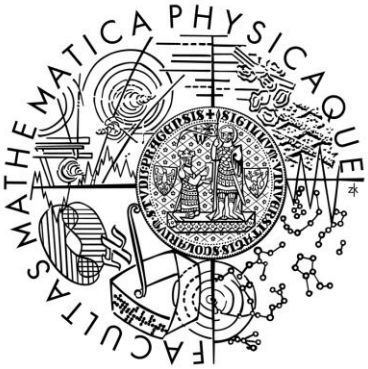

Klaudia Horváth

Vliv přímesových prvků a textury na plastickou deformaci protlačovaných hořčíkových slitin

Katedra fyziky materiálů

Vedoucí diplomové práce: Ing. Patrik Dobroň, Ph.D.

Studijní program: Fyzika

Studijní obor: Fyzika kondenzovaných soustav a materiálů

Praha 2015

Charles University in Prague

Faculty of Mathematics and Physics

MASTER THESIS

Klaudia Horváth

Effect of alloying elements and texture on plastic deformation of extruded magnesium alloys

Department of Physics of Materials

Supervisor of the master thesis: Ing. Patrik Dobroň, Ph.D.

Study programme: Physics

Specialization: Physics of condensed matter and materials

Prague 2015

I would like to express my gratitude to everyone who helped me during working on my thesis. First and foremost, many thanks go to my supervisor Ing. Patrik Dobroň, Ph.D. for his guidance, help, good advices and patience. My thanks must also go to doc. RNDr. Krisztián Máthis, Ph.D., who always managed to find some time to provide help and advice. I also thank very much to Dr. Jan Bohlen, for providing the access to X-ray diffraction measurements and for the diffraction data processing. My thanks go to Ing. Jana Kálalová and Marta Čepová for their help during experimental work and to Daria Drozdenko for her useful ideas. Last but not the least important, I owe more than tanks to my family members and friends for their support.

This work was completed within the framework of the research grant 13 - 19812S by the Czech Science Foundation.

I declare that I carried out this master thesis independently, and only with the cited sources, literature and other professional sources.

I understand that my work relates to the rights and obligations under the Act No. 121/2000 Coll., the Copyright Act, as amended, in particular the fact that the Charles University in Prague has the right to conclude a license agreement on the use of this work as a school work pursuant to Section 60 paragraph 1 of the Copyright Act.

In Prague 05/05/2015 Klaudia Horváth

Název práce: Vliv přímesových prvků a textury na plastickou deformaci protlačovaných hořčíkových slitin

Autor: Klaudia Horváth

Katedra / Ústav: Katedra fyziky materiálů

Vedoucí diplomové práce: Ing. Patrik Dobroň, Ph.D., Katedra fyziky materiálů

Abstrakt:
Práce je zaměřena na získání nových poznatků o vztahu mikrostruktury, textury a deformačních mechanismů v hořčíkových slitinách (Mg) bez příměsi hliníku. Slitiny s příměsí zirkonia, zinku, manganu a neodymu (ZK10, MN11, ZN11) ve formě extrudovaných profilů byly zkoumány při pokojové teplotě. Jednoosé tahové a tlakové zkoušky byly provedeny ve třech směrech: ve směru extruze (ED), v transverzálním (TD) a normálovém směru (ND). Ke studiu kolektivních dislokačních mechanismů a vzniku dvojčat byla využita metoda akustické emise. Vývoj deformační textury byl zkoumán pomocí rentgenové difrakce na vzorcích, které byly namáhány v tlaku do různého stupně deformace.

Klíčová slova: Mg slitina, deformační testy, akustická emise, textura

Title: Effect of alloying elements and texture on plastic deformation of extruded magnesium alloys

Author: Klaudia Horváth

Department / Institute: Physics of condensed matter and materials

Supervisor of the master thesis: Ing. Patrik Dobroň, Ph.D., Physics of condensed matter and materials

Abstract:
This work is focused on the study of the relationship between microstructure, texture and deformation mechanisms in aluminum-free magnesium (Mg) alloys. Extruded alloys containing zirconium, zinc, manganese and neodymium (ZK10, MN11, ZN11) in a form of rectangular profiles were deformed at room temperature. Uniaxial tensile and compression tests were performed in the extrusion (ED), transversal (TD) and normal direction (ND). The concurrent acoustic emission (AE) measurement was used in order to study the collective dislocation dynamic and the nucleation of twins. The deformation texture was studied by X-ray diffraction on samples deformed in compression up to different stress levels.

Keywords: Mg alloys, deformation tests, acoustic emission, texture

Contents

Introduction

In recent years, the reduction of air pollution by decreasing the fuel consumption is an important topic. The challenge can be achieved by using lighter materials in transport industry, thereby reducing the total weight. The aim is to replace the conventional materials retaining the mechanical properties.

Magnesium alloys belong to the lightest construction materials. Their density is lower than that of in industry used steels and aluminum alloys (Al). Mg alloys have high specific strength and stiffness. Another advantage of Mg is its easy availability (from 1 liter of seawater we can obtain 1.4 g Mg [1]) and good recyclability. Comparing to polymers, it has better mechanical properties and higher electrical and thermal conductivity.

The main limitation for their use is poor formability and ductility at ambient temperature, particularly low corrosion resistance, higher thermal expansion than that of Al alloys and weakening of their mechanical properties with increasing temperature (such as lower strength at temperatures above 200 °C [2]).

Limited ductility of Mg is linked with its hexagonal close packed structure (hcp). The deformation processes in hcp metals are not fully understood and therefore further studies are needed. One of the important parameters influencing their deformation processes is the ratio of crystallographic axes *c/a*. In Mg, the ratio is close to $\sqrt{\frac{8}{3}}$, what is the closest configuration of atoms in hcp lattice, and therefore, under certain conditions, besides primary basal slip, additional prismatic and pyramidal slip can be activated.

In the present work, the acoustic emission (AE) technique was used to study the deformation mechanisms of Mg alloys. AE is generated inside the material during plastic deformation and is closely related to deformation mechanisms and fracture processes in materials. The first systematic studies on AE were done in the 50s of the last century by Joseph Kaiser, who studied AE from metallic and non-metallic materials [3].

Objectives and scope

The majority of published papers are dealing with Mg alloys extruded into cylinder form, where the anisotropy of mechanical properties is "only" between the extrusion direction and the direction perpendicular to the axis of extrusion. The presented work is focused on new, perspective Mg alloys, which were extruded into the form of rectangular profiles. This method allows for the examination of the alloys in three directions: extrusion direction (ED), transversal direction (TD) and normal direction (ND).

The main aims of the thesis were to:

- Study the initial microstructure and texture of extruded profiles depending on the alloying (light microscope, X-ray diffraction)
- Investigate the microstructural stability (by light microscopy and microhardness measurements)
- Examine the deformation behavior of the extruded profiles (tension and compression tests)
- Study the anisotropy and the tension-compression yield strength asymmetry of the profiles
- Clarify the role of twinning during deformation (acoustic emission, X-ray diffraction)

1. Theory

1.1. Plastic deformation of metals with a hexagonal close packed crystal structure

We talk about plastic deformation, when a material undergoes non-reversible changes of shape in response to applied force [4]. In generally, plastic deformation in metals with a hexagonal close packed crystal lattice (hcp) is realized by dislocation glide and twinning. Dislocation glide is dislocation motion along a definite crystallographic plane, whereby in twinning only a small movement of atoms occurs and this process is more quickly than slip. Dislocations belong to the line defects in crystalline materials and exist in two primary types; edge (Fig. 1.1a) and screw (Fig. 1.1b) dislocations. The generation and interaction of dislocations can significantly influence deformation behavior of crystalline materials.

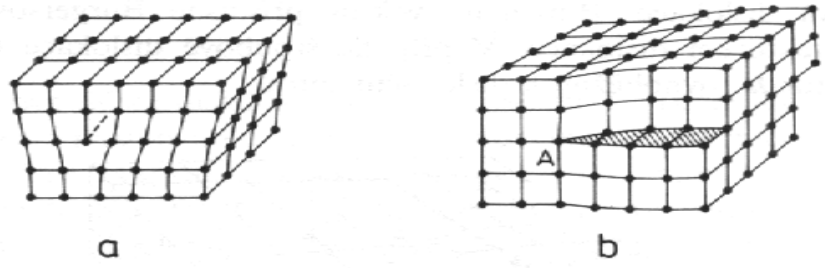

Fig. 1.1. Edge (a) and screw (b) dislocation [5]

The plastic deformation of polycrystalline materials (polycrystals) in comparison to single crystals is strongly affected by grain boundaries (behave like obstacles for dislocation movement) and the orientation of grains [6]. Deformation in polycrystals starts in those grains, which are most favorable oriented for slip with respect to the applied stress.

The characteristic values of the plastic deformation are ductility and strength of the material. The ductility is expressed through the elongation on the contraction to the fracture. The yield strength (YS) is the stress corresponding to the strain of 0.2 %. Macroscopic plastic deformation starts after reaching the YS. The ultimate strength (σ_m) is the maximum stress which the material can reach before its fracture.

1.1.1. Slip systems in hcp crystal lattice

Generally, in the hcp metals three main slip systems: the basal, prismatic and pyramidal can be distinguished (Fig. 1.2). Their activation strongly depends on the ratio of the crystallographic axis *c* to *a* (Fig. 1.3). The ideal ratio *c/a*, i.e. the closest configuration of atoms in hcp lattice, is equal to $\sqrt{\frac{8}{3}}$. If the ratio is greater than the ideal value, slip takes place primary in the basal plane with the highest density of atoms (e.g. Zn, Cd). If this ratio is lower than the ideal value, slip takes places in the prismatic and pyramidal slip systems (e.g. Ti). In the case of Mg, the *c/a* ratio is close to $\sqrt{\frac{8}{3}}$ and therefore, under certain conditions, besides the primary basal slip, additional prismatic or pyramidal slip can be activated. The highest impact on their activation in Mg can be attributed to the deformation temperature.

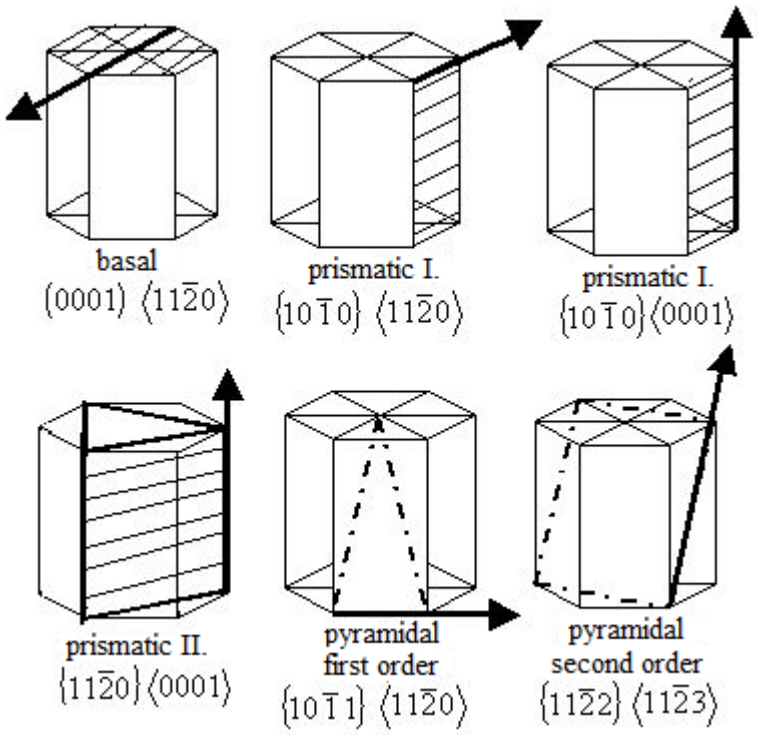

Fig. 1.2. Basic slip systems in materials with hcp lattice [8]

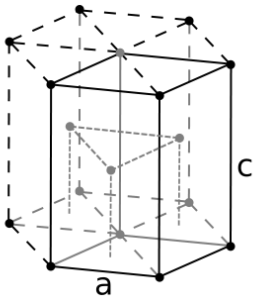

Fig. 1.3. Hexagonal lattice

According to the von Mises criterion [7], the compatible plastic deformation in polycrystalline material requires at least 5 independent slip systems. In Mg and its alloys there are available only two crystallographically independent easy slip systems at room temperature (RT). The main slip system is the basal (0001) plane with the highest density of atoms in direction $\langle 11\bar{2}0 \rangle$ and the lowest critical resolved shear stress (CRSS) of all slip systems.

Basal slip system does not allow deformation along the *c* axis and for the activation of pyramidal slip system at RT, a very high CRSS is required (approximately two orders of magnitude higher than for basal slip), what leads to the activation of an additional deformation mechanism, which is called twinning.

1.1.2. Twinning in Mg and its alloys

Twinning is the process when a part of the crystal is shifted to a new position, which is the mirror image of the original and the mirror plane is the twinning plane (Fig. 1.4). Twinning is caused by a stress concentration, e.g. from accumulated dislocations at grain boundaries. Nucleation of twins is homogeneous and depends on the microstructure [9]. This phenomenon contributes to increasing the dislocation density, which leads to the strain hardening of the material [10].

The formation of twins depends not only on the applied stress but also on temperature and on the grain size. With increasing temperature the CRSS for the activation of non-basal slip systems decreases and therefore above a certain temperature twinning is not required anymore.

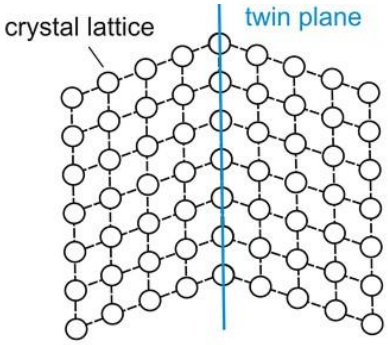

Fig. 1.4. Twin plane [11]

The main twinning system in Mg alloys is $\{10\bar{1}2\}\langle 10\bar{1}1\rangle$ system, which is also called extension twin due to the elongation of the crystal along the c-axis. This type of twinning can be activated by tension along the c-axis or by compression perpendicular to the c-axis. During the $\{10\bar{1}2\}\langle 10\bar{1}1\rangle$ twinning the crystal lattice is rotated around the $(10\bar{1}2)$ plane and the re-orientation angle between the mother grain structure and the new created twin is 86.3° (Fig.1.5). The other important twinning systems are the $\{10\bar{1}1\}\langle 10\bar{1}\bar{2}\rangle$ systems, so called compression twins (shortening in crystal along the c-axis).

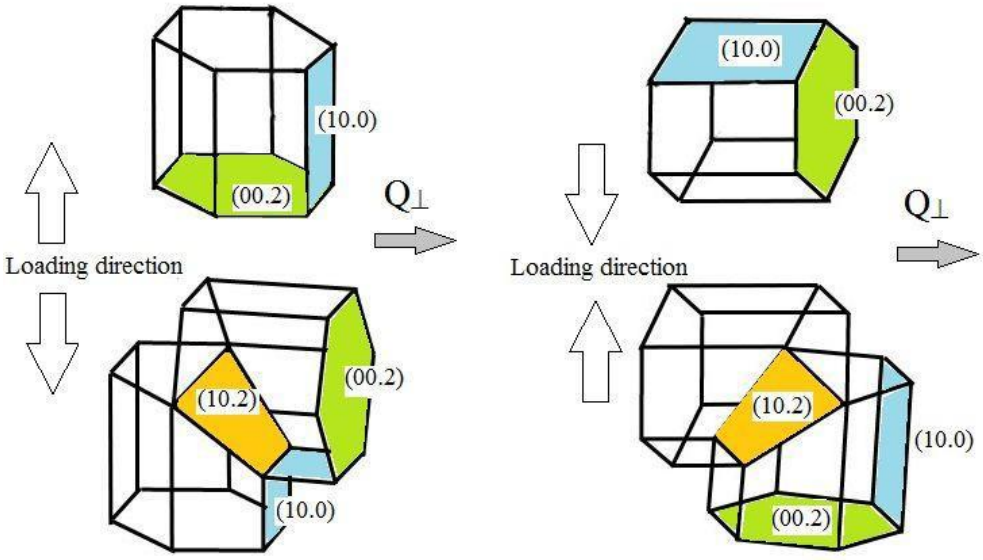

Fig. 1.5. Dependence of twinning mechanisms on the loading direction
a) tension, b) compression [12]

1.2. Extrusion

Extrusion is a process which is used to manufacture semi-finished and final products. The principle of the extrusion is shown in Fig. 1.6. During the forward (direct) extrusion (Fig. 1.6 left), the material flows in the direction of the extruder while to achieve a uniform pressure on the walls of extruded material a hydrostatic medium is applied. In the backward (indirect) extrusion (Fig. 1.6 right), a material flows against the working direction of the extruder without the use of a hydrostatic medium.

The final grain size depends on process parameters, such as temperature and extrusion speed. An advantage of the hydrostatic extrusion against the backward extrusion is in a uniform applied pressure on the surface of the material. Furthermore, there is no direct contact of the material with the tool and therefore such arrangement does not produce any cracks on the surface of the extruded profile. In view of this fact, for hydrostatic extrusion process higher compression ratio could be used and in a material finer microstructure can be achieved [13].

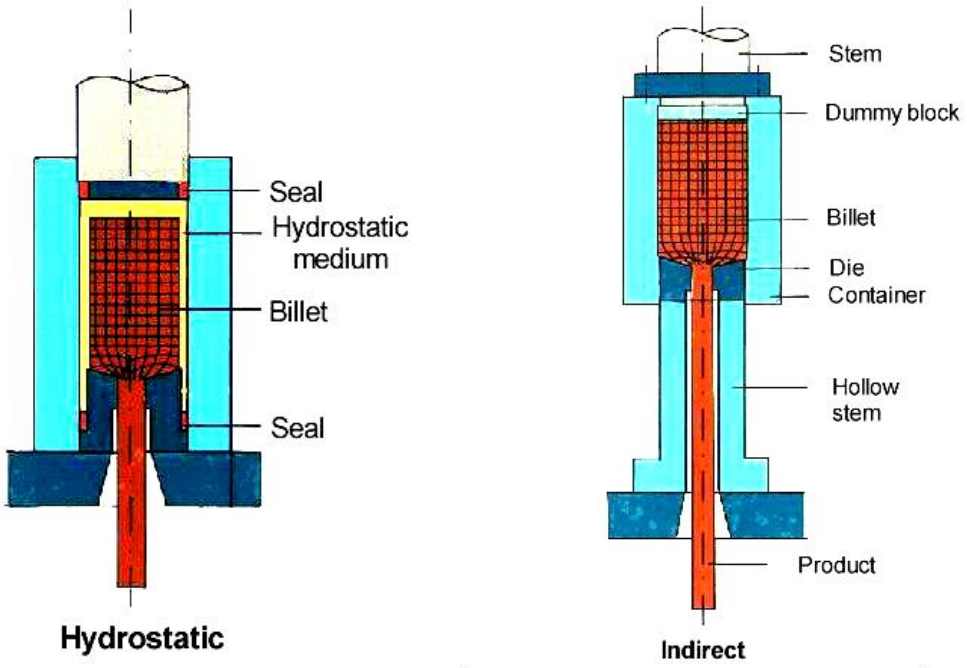

Fig. 1.6. The principle of forward (hydrostatic) and backwards (indirect) extrusion [14, 15]

1.3. Wrought magnesium alloys

The wrought Mg alloys have better mechanical properties than the cast alloys; e.g. higher ultimate tensile strength [16] or better fatigue resistance [17]. The forming (extrusion, rolling) of Mg alloys leads to a development of a strong deformation texture (preferable grain orientation [18]), which is responsible for the asymmetry and anisotropy of mechanical properties, especially at RT [19, 20]. The activation of various deformation mechanisms (basal slip, twinning, prismatic slip, etc.) in wrought Mg alloys depends mainly on deformation texture, loading direction and temperature.

Extruded Mg alloys usually exhibit the orientation of basal planes nearly parallel to the ED. This texture is favorable for activation of the $\{10\bar{1}2\}\langle 10\bar{1}1\rangle$ twinning systems, which leads to lower YS in compression than in tension [21]. Weaker texture can reduce the tension-compression asymmetry at the YS, however also leads to lower values of the YS [22].

The microstructure of Mg alloys can be controlled by alloying. An addition of zirconium significantly improves the mechanical properties of extruded Mg alloys. Zirconium contributes to the grain refinement, what leads to high tensile strength without any significant decrease in ductility [23]. Another benefit of Zr addition is in the improved corrosion resistance [24].

Nascimento et al. in [25] compared extruded ZN11 and AZ31 alloys with a circular cross-section. The AZ31 alloy has inhomogeneous microstructure with a strong texture, which is responsible for the high tension-compression asymmetry at the YS. The asymmetry is associated with a high twinning activity during compression. The ZN11 alloy exhibits a fully recrystallized (homogeneous) microstructure with a weak texture, what results in the elimination of the asymmetry at the YS.

Mg–Mn alloys have potential for applications due to their good castability, tensile strength and hardness, as well as improved corrosion resistance [22]. Recent study of the MN11 alloy has shown [26] that the RE content in Mg alloys has high influence on the CRSS values. Mainly, the CRSS for the basal slip and for twinning is affected in the way that the ratio of $CRSS_{basal}$ / $CRSS_{twinning}$ is increasing while the ratios of $CRSS_{prismatic}$ / $CRSS_{twinning}$ and $CRSS_{pyramidal}$ / $CRSS_{twinning}$ are decreasing. It

was also shown in [20] that the MN11 alloy has a very weak texture with basal planes tilted away from the ED.

1.4. Acoustic emission

1. 4. 1. Definition and method of acoustic emission

Acoustic emission (AE) is defined as transient elastic waves, which are generated by a sudden release of energy due to local dynamic changes in the material [27].

AE is also a diagnostic method based on this phenomenon. AE belongs to the passive non-destructive methods, which gives real time (*in-situ* measurement) and integral information from entire volume about the dynamic state of the material. Disadvantage of the AE method is given by a complex character of AE signals and the low energy signals can be hidden in the background noise [28].

1. 4. 2. The sources of acoustic emission

The source of AE is a local process which produces detectable AE signals. The AE signal is a single dynamic process which is caused by a rapid release of a certain amount of energy [29].

Depending on the character of elastic waves, two types of AE can be distinguished (Fig. 1.7):

- Continuous emission – elastic waves from large number of sources with a low energy,
- Burst emission – AE signals have the character of time separated pulses with a high energy.

The interaction (annihilation, intersection) and the accumulation of dislocations at obstacles, or unpinning from the obstacles lead to continuous AE [30]. Continuous AE also occurs during recrystallization or martensitic phase transformation [31].

The burst AE can be produced by the unstable fashion of plastic deformation, nucleation and propagation of cracks, fracture or corrosion phenomena. The released energy may be 10 to 14 orders of magnitude greater than in continuous AE [32].

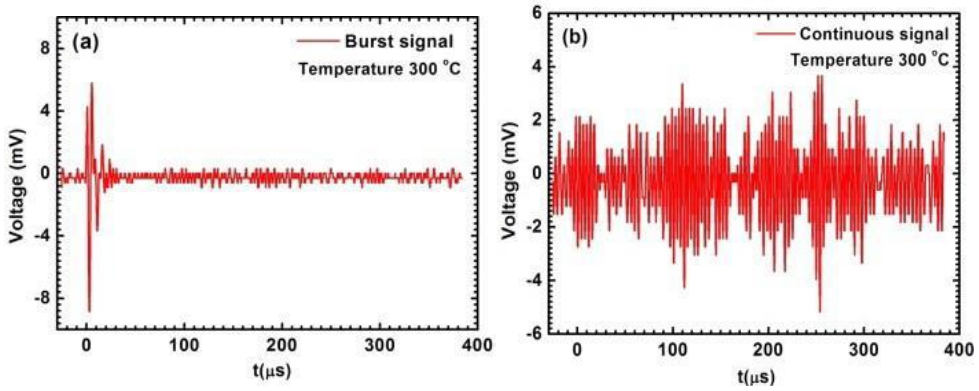

Fig. 1.7. Burst (left) and continuous (right) AE [33]

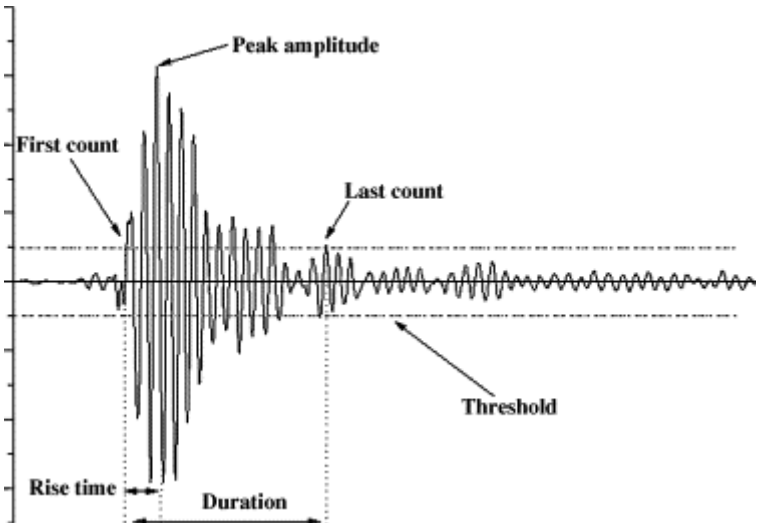

Fig. 1.8. Characterization of burst AE [34]

1. 4. 3. Terminology and basic parameters of AE

- AE signal – an electrical signal obtained by the detection of one or more AE events. The signal is described by its amplitude, shape, rise time, duration, energy and its spectrum.
- AE signal start - the beginning of an AE signal as recognized by the system processor, usually defined by an amplitude excursion exceeding threshold.
- AE signal end - the recognized termination of an AE signal, usually defined as the last crossing of the threshold by that signal.

- AE signal duration - the time between AE signal start and AE signal end.
- AE signal rise time - the time between AE signal start and the peak amplitude of that AE signal.
- Dead time - any interval during data acquisition when the instrument or system is unable to accept new data for any reason.
- AE event – a local material change giving rise to AE.
- Emission oscillation – shape of emission signal in one period of such frequency which has the maximum amplitude (peak amplitude) of the entire spectrum.
- AE count – the number of times the acoustic emission signal exceeds a threshold (Fig. 1.8).
- AE count rate – the number of the emitted pulses with amplitude greater than the threshold per a unit time.
- AE event rate – the number of the events during a unit time. [35]

1. 4. 4. Detection of AE

The standard setting for measuring the AE activity is schematically shown in Fig. 1.9.

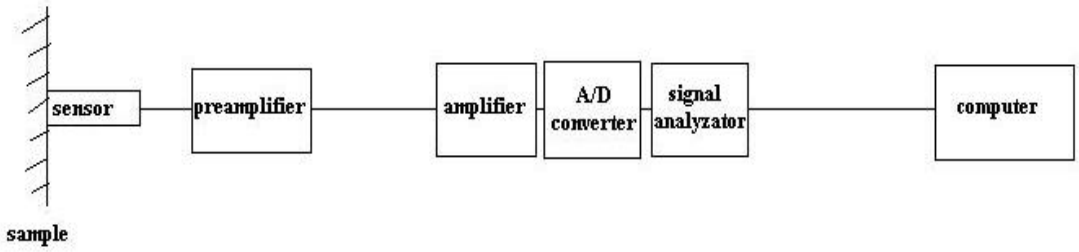

Fig. 1.9. Scheme of the detection of AE

The AE signal is usually detected by piezoelectric sensors, which are sufficiently sensitive and have relatively low price. Piezoelectric sensors are often made from a ceramic like lead zirconate titanate (PZT). There are two types of detectors. The resonance type detector is the most sensitive around the resonant frequency. The broad-band sensor has a flat response in a wide frequency interval

but is less sensitive. The typical working frequency is between 50 kHz and 1 MHz. The sensitivity of the sensor is defined in logarithmic scale by the equation:

$$dB_{AE} = 20\log\left(\frac{U}{U_r}\right) \quad (1),$$

where U_r is the reference voltage and it is equal to 1 μV.

Preamplifier is used to keep a high ratio between the detected signal and the background noise. The signals with low frequencies are filtered out because they could be affected by a noise of various natures (friction, vibrations from the machine, etc).

The A/D converter makes from the analogue data the digital one, while the data are time and amplitude separated. The sampling frequency determines how many values from the analog signal will be recorded per second.

The parameterization of the AE signal is usually based on the threshold level detection, what allows distinguishing between high and low amplitude signals. To separate individual AE events from the raw signal, set of parameters (e. g. threshold level, rise time, dead time) can be used.

2. Experimental methods

2. 1. Deformation tests

The tension and compression tests were performed in a universal testing machine INSTRON® 5882. The scheme of tensile test with concurrent AE measurement is shown in Fig. 2.1. For tensile testing, samples with a diameter of 8 mm and active length of 13 mm were prepared. The tensile tests were performed in the ED and TD. The shape of the materials did not allow producing tensile samples in the ND. The sample size for compression test is presented in Table 1. All deformations tests were carried out at room temperature (RT) with a constant strain rate of 10^{-3} s^{-1}. The measured data was recorded by using Blue Hill® supplied by INSTRON® for the testing machine.

Material	Direction	Thickness [mm]	Width [mm]	Length [mm]
ZN11 (Mg-Zn-Nd)	ED	11.8	12.3	9.4
	TD	9.7	11.5	12.4
	ND	12.4	11.6	9.6
MN11 (Mg-Mn-Nd)	ED	10.3	11.2	9.8
	TD	9.6	10.2	11.3
	ND	11.3	10.3	10.0
ZK10 (Mg-Zn-Zr)	ED	9.8	12.2	10.0
	TD	13.0	12.0	9.7
	ND	12.2	9.8	9.7

Table 1. The samples sizes for compression tests

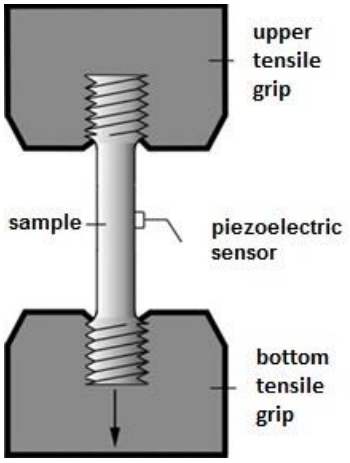

Fig.2.1. Scheme of tensile test with concurrent AE measurement

The compression tests of the ZK10 alloy, used for a study of texture evolution, were done in a universal testing machine Zwick® Z50 in Geesthacht, Germany.

All mechanical data were processed by program Origin® from the company OriginLab®.

2. 2. The acoustic emission measurements

AE was detected by computer-controlled system MICRO-II developed by Physical Acoustic Corporation (PAC), which allows a continuous storage of AE signals with a sampling frequency of 1 MHz. A preamplifier of 40 dB was used in order to keep a high ratio between AE signal and a noise. The threshold level was set to 26 dB. A piezoelectric sensor MIDI-410-61 (ZD RPETY-DAKEL) with a diameter of 6 mm was used (Fig. 2.2). AE Sensor was attached on the sample with a help of a clamp and to improve the contact between the sample and AE sensor, silicone grease was used.

Fig. 2.2. MIDI sensor for AE measurements [36]

2. 3. Light microscopy

Samples were cut along the ED and TD; i.e. the planes perpendicular to the ND were investigated, using a machine Accutom-50 from Struers®. The samples were mounted by ClaroCit and then they were wet grinded with TegraPol-15 from Struers® on SiC grinding papers from P800 to P4000. In addition, they were polished by a diamond paste with a size of 3, 1 and ¼ μm. The polished surfaces were firstly etched with 5% Nithal for 5 s and then with an etchant (50 ml of ethanol, 9 ml of water, 4 ml of an acetic acid and 6 g of a picric acid (98%)) for 10 s.

The microstructure was investigated by the OLYMPUS GX51 microscope equipped with the PIXELINE® camera. The obtained microstructures were evaluated using the software from NIS – Elements AR®.

2. 4. Energy dispersive X-ray analysis (EDAX)

EDAX was used for the determination of the chemical composition of Mg alloys. The X-rays, produced by the interaction of the electron beam with the sample, were detected by the FEI QUANTA 200 FEG scanning electron microscope. The primary electron beam was accelerated by the accelerating voltage of 20 kV. The samples were grinded and polished in a way introduced in Chap. 2.3 and the detection was done in a plane, which is perpendicular to the ED.

2. 5. Texture measurements

For a study of crystallographic texture in the Mg alloys, X-ray diffraction was used. Texture measurements were done in Germany at Magnesium Innovation Centre, Helmholz-Zentrum Geesthacht using a diffraction machine TCU 150 Anton Paar from PANalytical. The CuK_{α} radiation with a beam size of 2x1 mm was used. The texture was measured on polished surfaces (see chap. 2.3), which were perpendicular to the ED. The data were processed by program MatLab produced by MathWorks.

2. 6. Microhardness measurement

Microhardness was measured by QNess Q10A + aperture. HV 0.05 setting was used, what means that a force of 0.5 N is applied for 10 s and the indentions were evaluated by a lens with the 65x optical zoom. Samples were cut by machine Accutom-50 from Struers® into a cubic form with a dimension approximately of (10 x 10 x 10) mm. The sample surfaces were grinned and polished. More details about the sample preparation can be found in Chap. 2.3. The microhardness maps (square grid of 15x15 points) were done with a step size of 0.25 mm.

3. Results

3. 1. Experimental materials

In the present work the MN11, ZN11 and ZK10 magnesium alloys were investigated. Their chemical composition was determined by EDAX and the measured values with production conditions are listed in Table 2. The materials were prepared in Magnesium Innovation Centre, Helmholtz - Zentrum Geesthacht (Germany) by gravity casting and extrusion through a rectangular section of dimensions 100 x 11 mm into the final form.

	Chemical composition				**Extrusion speed (mm/s)**	**Extrusion temperature (°C)**
	Zn (wt. %)	**Mn (wt. %)**	**Nd (wt. %)**	**Zr (wt. %)**		
MN11	**-**	**1.10**	**0.79**	**-**	**3.3**	**350**
ZN11	**1.03**	**-**	**0.83**	**-**	**3.3**	**350**
ZK10	**0.94**	**-**	**-**	**0.14**	**10**	**250**

Table 2. Chemical composition and production conditions of the Mg alloys

The microstructure, texture represented by pole figures and grain size distribution of investigated materials are shown in Figs. 3. 1 – 3.3.

The MN11 alloy exhibits a homogeneous polyhedral microstructure with the average grain size of 17 ± 7 μm (Fig. 3.1). A relative strong texture with basal planes nearly parallel to the ED and perpendicular to the ND is observed. In the (0001) pole figure, the basal planes are split towards the ED and exhibit two distinct maxima.

In ZN11 alloy, a polyhedral fine-grained microstructure with the average grain size of 12 ± 4 μm (Fig. 3.2) was found. The alloy shows a relatively weak texture with basal planes parallel to the ED. In the (0001) pole, similarly to the MN11 alloy, higher spread of the basal planes towards the ED than towards the TD was found.

The ZK10 alloy has an inhomogeneous polyhedral microstructure and the grain size varies from 5 up to 60 μm (Fig. 3.3). The alloy exhibits a strong texture with basal planes parallel to the ED and perpendicular to the ND.

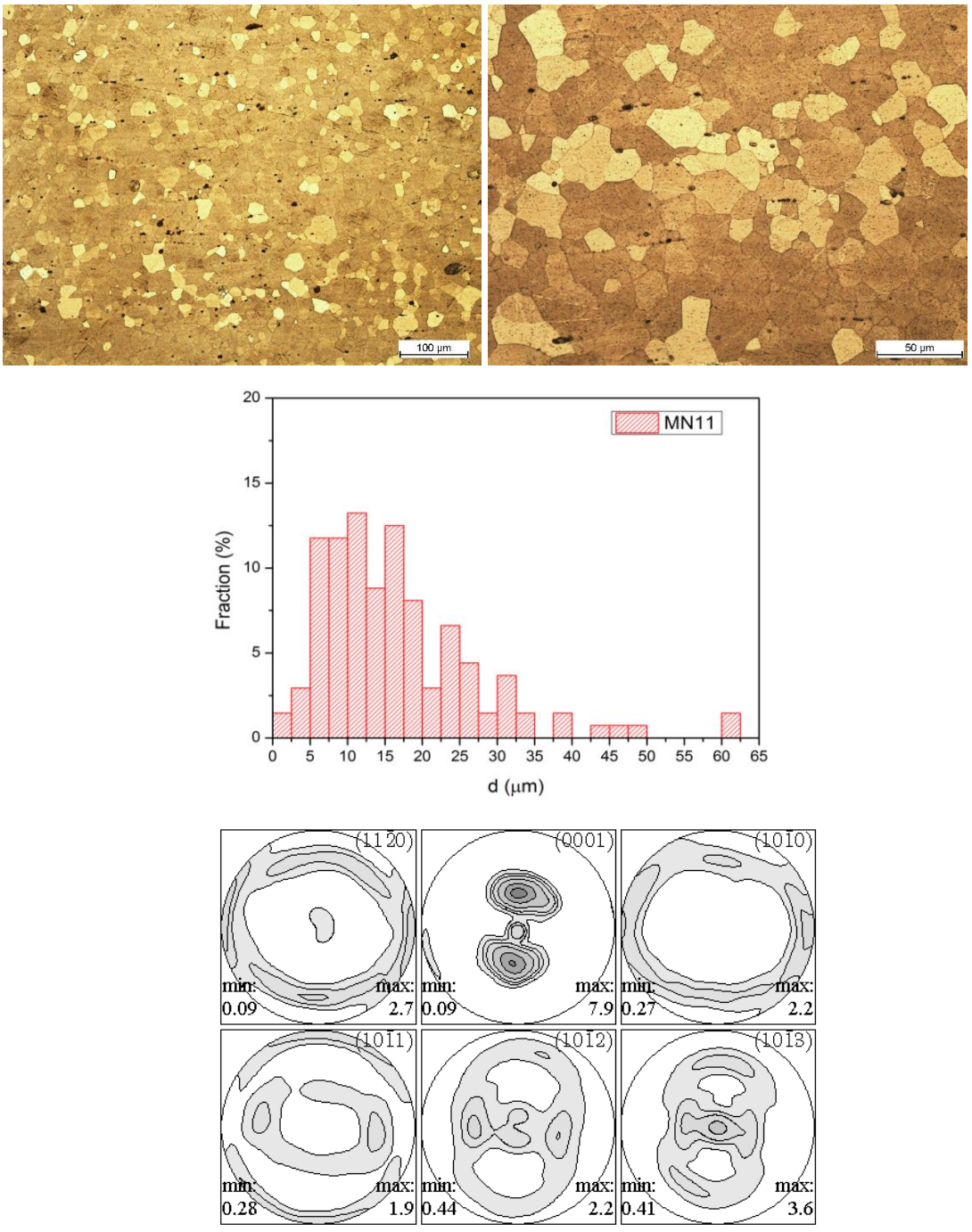

Fig. 3.1. Microstructure (ED→), texture (ED↑, TD→) and grain size distribution of MN11 alloy

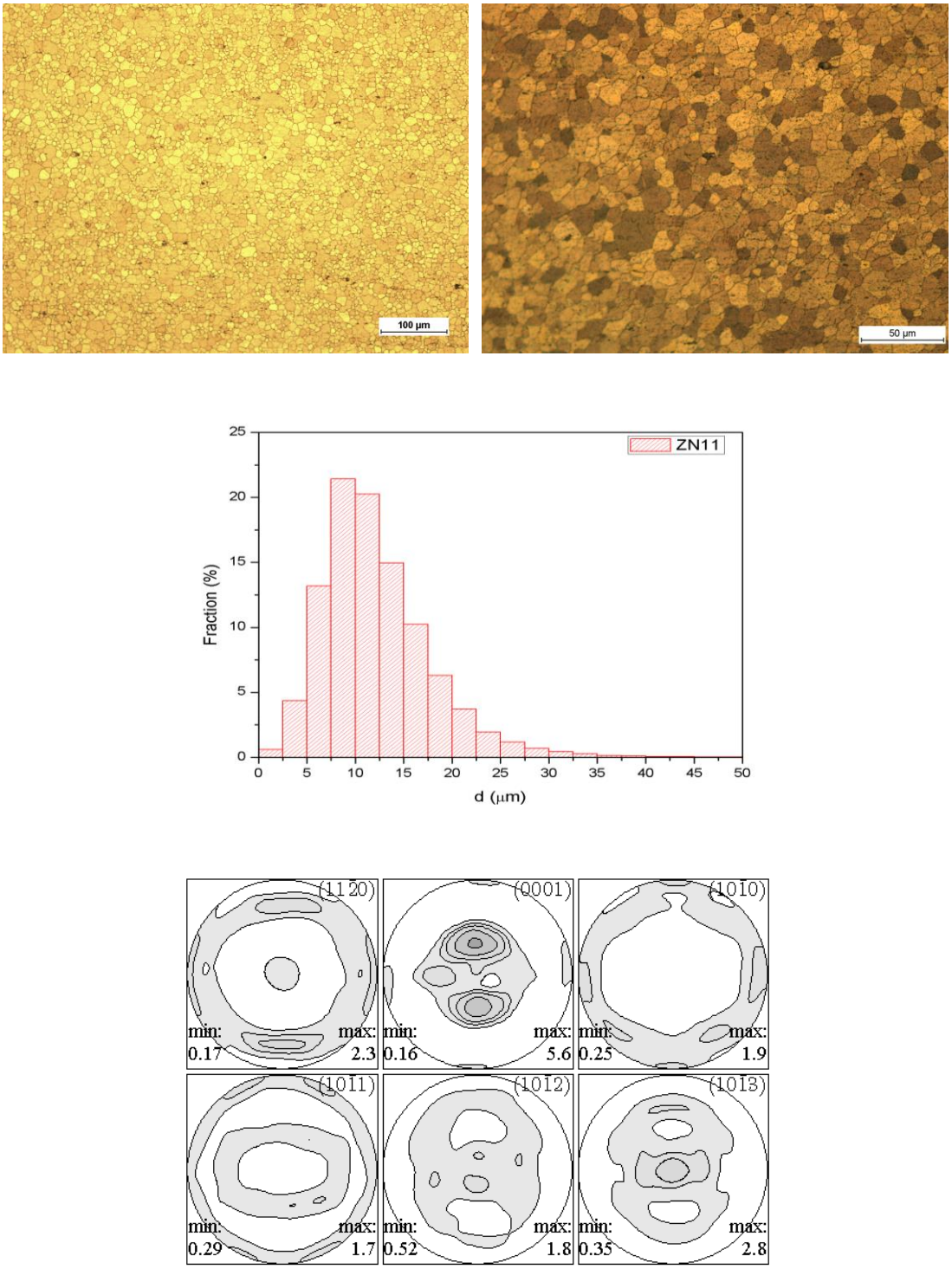

Fig. 3.2. Microstructure (ED→), texture (ED↑, TD→) and grain size distribution of ZN11 alloy

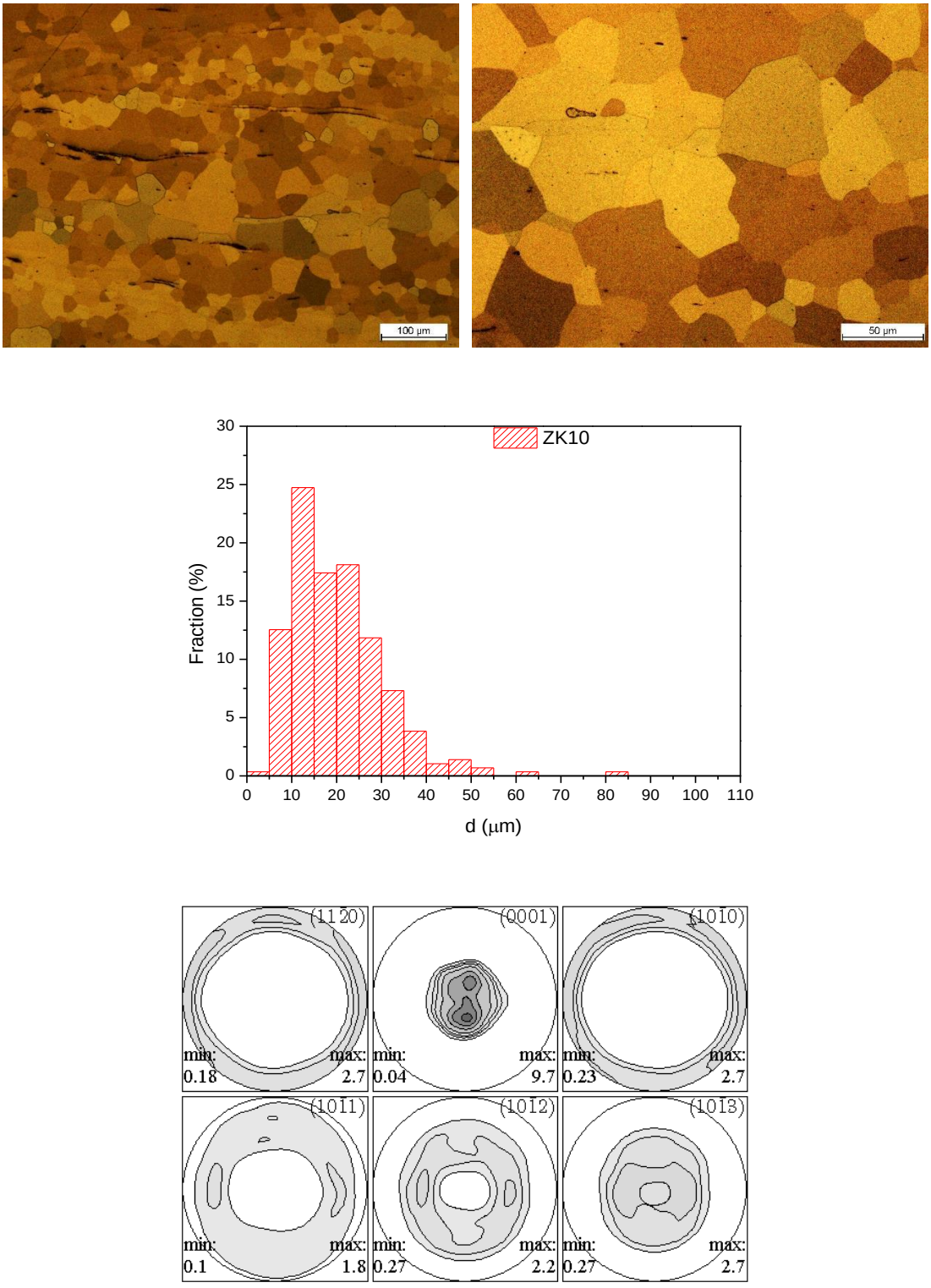

Fig. 3.3. Microstructure (ED→), texture (ED↑, TD→) and grain size distribution of ZK10 alloy

In order to study the stability of the microstructure, the samples were annealed at 300 °C for a various time. Heat treatment can influence the microstructure, especially if recrystallization processes occur, which can significantly influence the mechanical properties of Mg alloys. The dependence of the microhardess on the annealing time is plotted in Fig. 3.4, where the average values with corresponding error bars were calculated from 255 measured points. The microhardness slightly decreases with increasing annealing time however with respect to error bars, the microhardness can be considered constant throughout the annealing time interval of (1 – 10) hours.

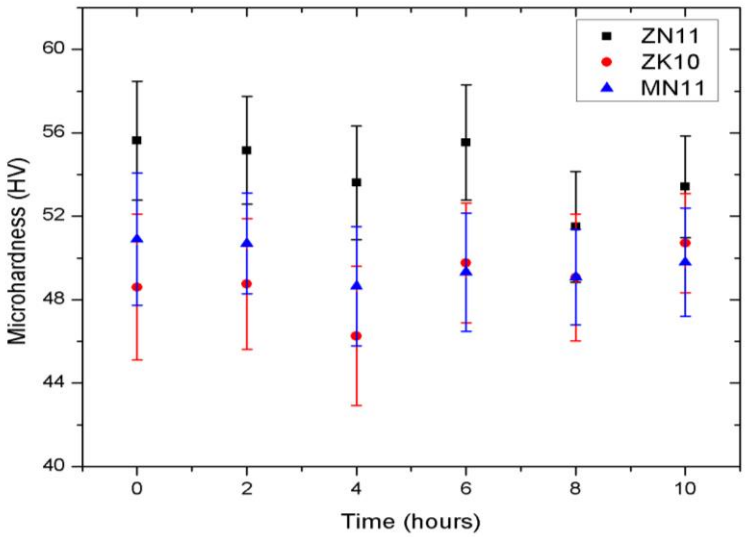

Fig. 3.4. Microhardness of the ED surface vs. annealing time (at 300 °C)

Furthermore, the ZK10 alloy was annealed at 300 °C for 20 hours in order to prove the stability of microstructure. The microstructure and the texture after annealing for 10 and 20 hours are shown in Figs. 3.5 and 3.6, respectively. After annealing for 10 hours, some grains are elongated towards the ED and the average grain size increases by comparison with the non-annealed ZK10 alloy. The small amount of twins in the microstructure is the result of sample preparation. After annealing for 20 hours, the microstructure is fully recrystallized and homogeneous (Fig. 3.6). The annealing process did not significantly influence the texture of the material and therefore basal planes remain parallel to the ED.

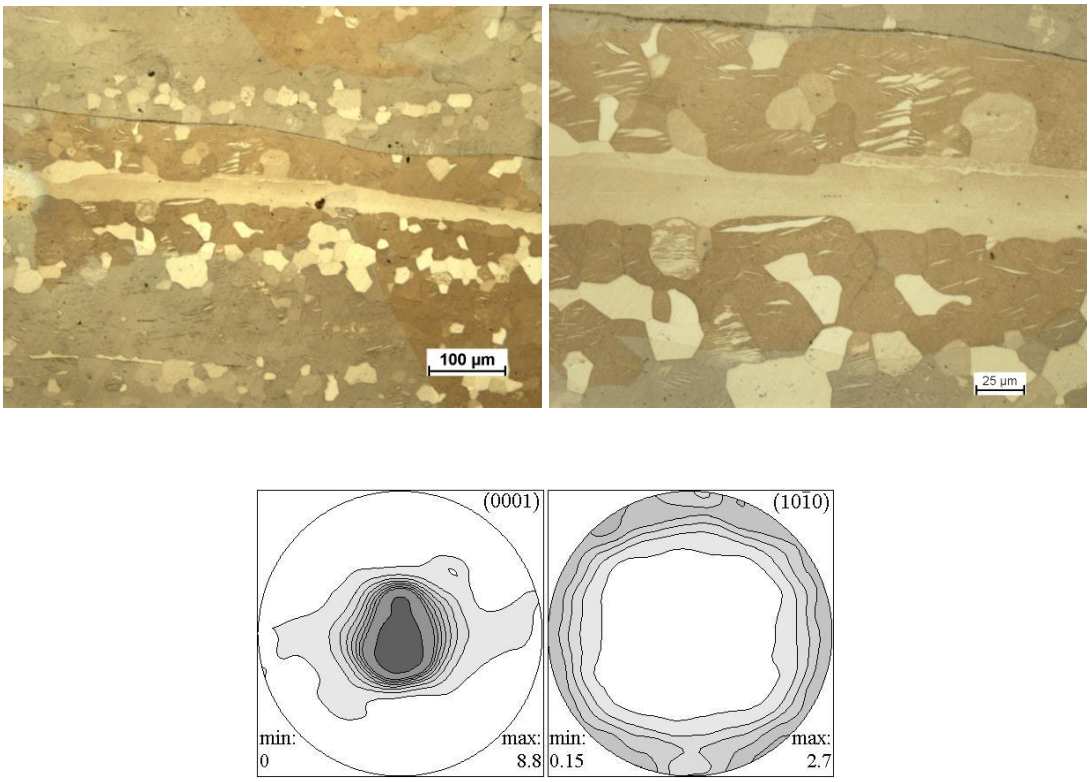

Fig. 3.5. Microstructure (ED→) and texture (ED↑, TD→) of ZK10 alloy after annealing at 300 °C for 10 hours

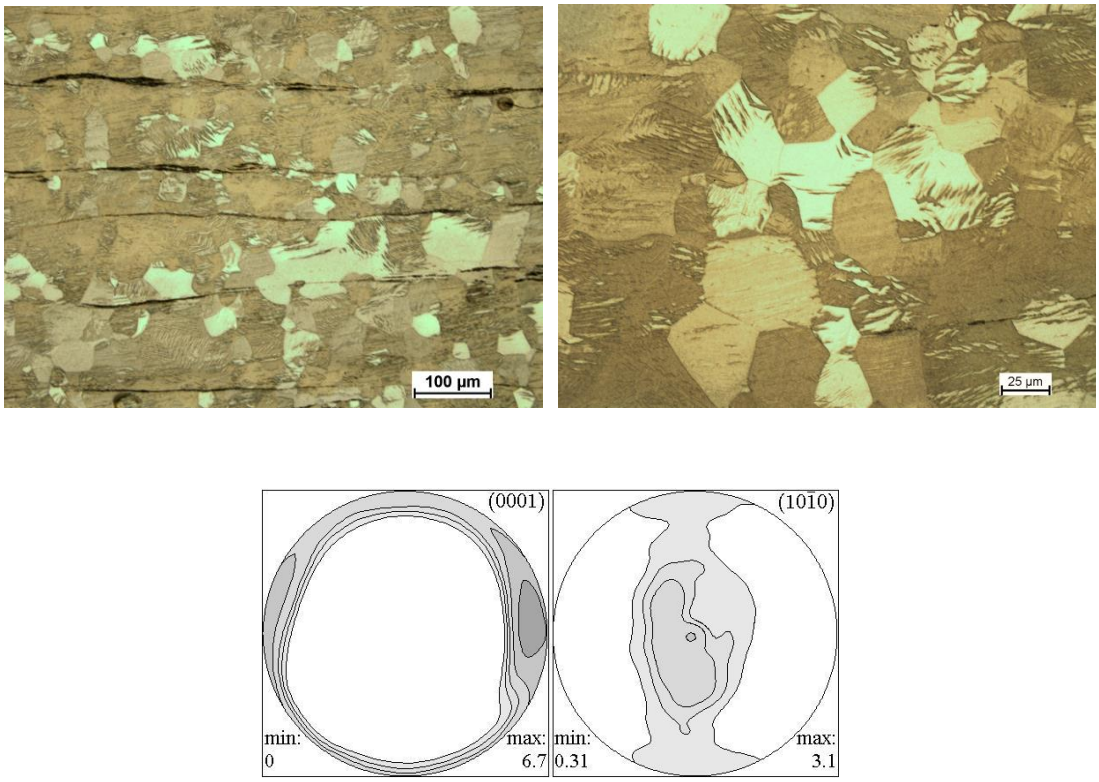

Fig. 3.6. Microstructure (ED→) and texture (TD↑, ND→) of ZK10 alloy after annealing at 300 °C for 20 hours

Moreover, the ZK10 alloy was annealed at 400 °C for 2, 6 and 10 hours in order to study the evolution of microstructure. The annealing process did not significantly change the microstructure and the grain size is almost constant. The results after annealing for 10 hours are shown in Fig. 3.7.

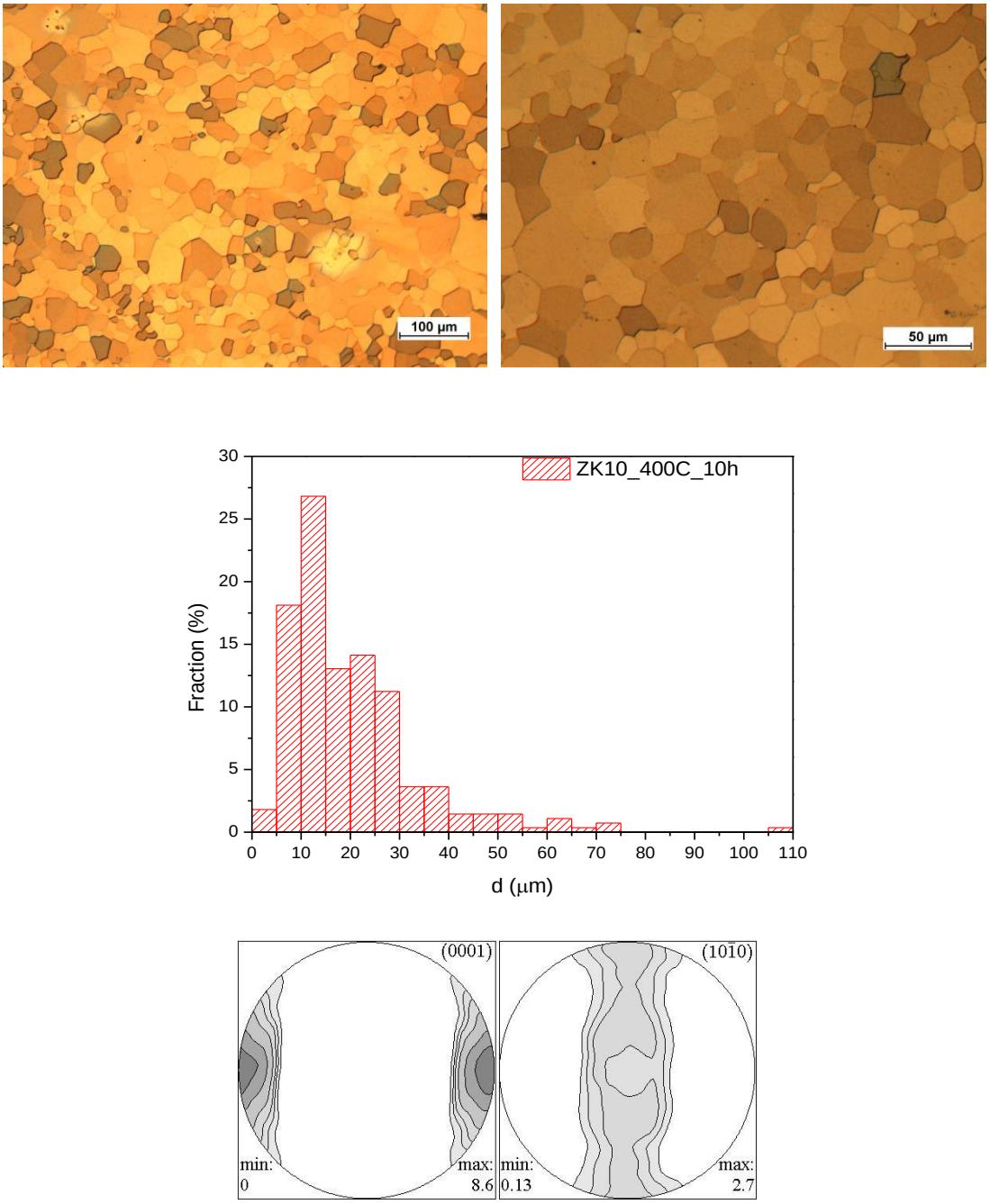

Fig. 3.7. Microstructure (ED→) and texture (TD↑, ND→) of ZK10 alloy after annealing at 400 °C for 10 hours

3. 2. Deformation tests

Tensile true stress - strain curves for the orientation of the load axis along the ED and TD (ED and TD samples) are shown in Figs. 3.8 – 3.10. All curves exhibit a typical shape for polycrystalline materials with a linear part at the beginning of the test, what corresponds to elastic deformation. In the MN11 (Fig. 3.8) and ZN11 alloys (Fig. 3.9), the YS and ultimate tensile strength (UTS) are higher for the TD than for ED sample. In the MN11 alloy, the elongation to failure is comparable for both the ED and TD samples, whereas in the ZN11 alloy higher ductility was found in the ED sample. In the ZK10 alloy (Fig. 3.10), the YS is comparable for both ED and TD samples. Higher elongation to failure in the ED than in the TD sample was measured.

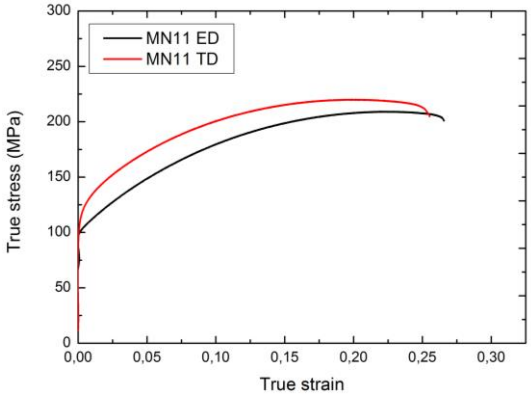

Fig. 3.8. Tensile tests of MN11 alloy

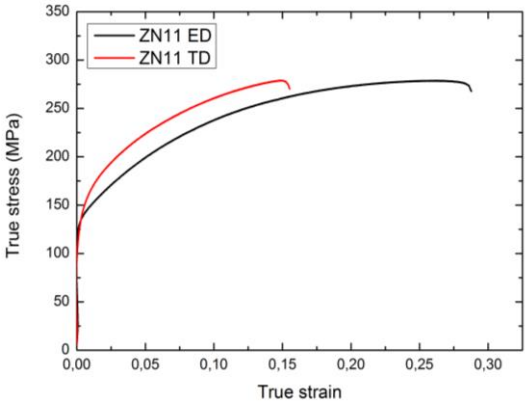

Fig. 3.9. Tensile tests of ZN11 alloy

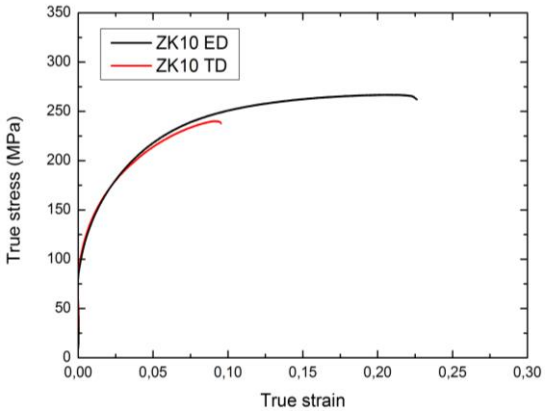

Fig. 3.10. Tensile tests of ZK10 alloy

True stress – strain curves in compression for all three directions (ED, TD, ND) are shown in Figs. 3.11 – 3.13. In all three Mg alloys deformed along the ED and TD, S-shaped compression curves were observed. The shape of compression curve for the ND sample is similar to tensile curves for the ED and TD samples (Figs. 3.8 – 3.10). Therefore, the highest YS for the ND sample by comparing with the ED and TD samples were found in all Mg alloys. In MN11 (Fig. 3.11) and ZN11 (Fig. 3.12) alloys, the lowest YS is in the ED sample. In the ZK10 alloy (Fig. 3.13), the lowest YS were found in both ED and TD samples. The highest ultimate compression strength (UCS) from all three directions was measured in the TD sample for the MN11 and ZN11 alloys, while in the ZK10 alloy, it was observed in the ED sample. In the MN11 alloy, the ductility is very similar for all three directions. In the ZN11 and ZK10 alloys, the highest elongation to failure is measured in the ND sample and the smallest one is found in the TD sample. By comparing all three Mg alloys, the ZN11 alloy exhibits the best ductility.

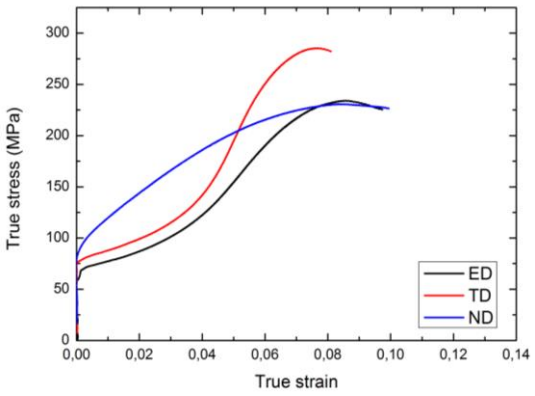

Fig. 3.11. Compression tests of MN11 alloy

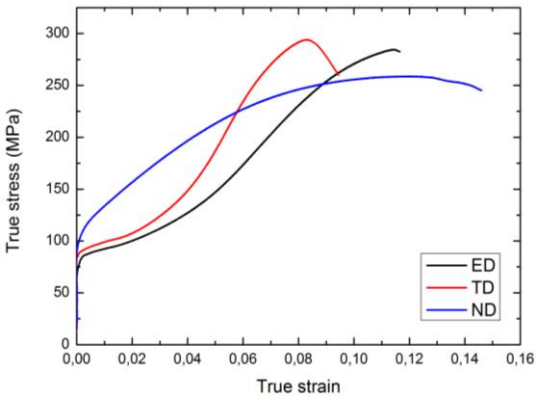

Fig. 3.12. Compression tests of ZN11 alloy

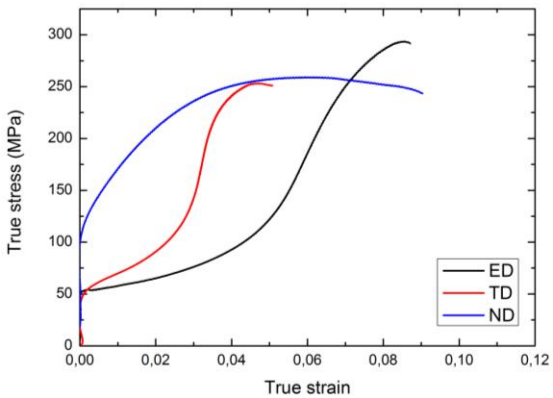

Fig. 3.13. Compression tests of ZK10 alloy

The YS values for both compression and tension are shown in Fig. 3.14. The smallest tension-compression YS asymmetry is detected for the MN11 alloy deformed along the ED. The highest asymmetry is measured in the same alloy deformed along the TD. For the ZN11 alloy, the asymmetry in the ED sample is slightly lower than in the TD sample. In the ZK10 alloy, the YS asymmetry is higher in the ED than in TD sample.

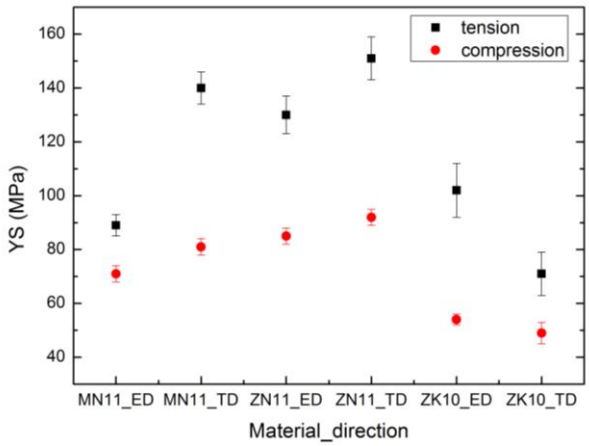

Fig. 3.14. Tension-compression asymmetry at the yield point

3. 3. Acoustic emission measurements

The time dependence of the tensile stress, the AE count rate and the AE signal for the MN11 alloy deformed along the ED and TD is plotted in Fig. 3.15 and 3.16, respectively. Stronger AE signal (higher amplitudes) are measured during deformation along the TD. The highest amplitudes are observed at the onset of plastic deformation before the YS. The maximum of the AE count rate can be related to the macroscopic yield point and higher value can be seen in the ED than in the TD sample. After the YS, the AE activity decreases with increasing plastic deformation. This decrease is more pronounced for the TD than for ED sample. It is interesting to note that while the AE count rate is higher in the ED sample, the AE signal is stronger in the TD sample.

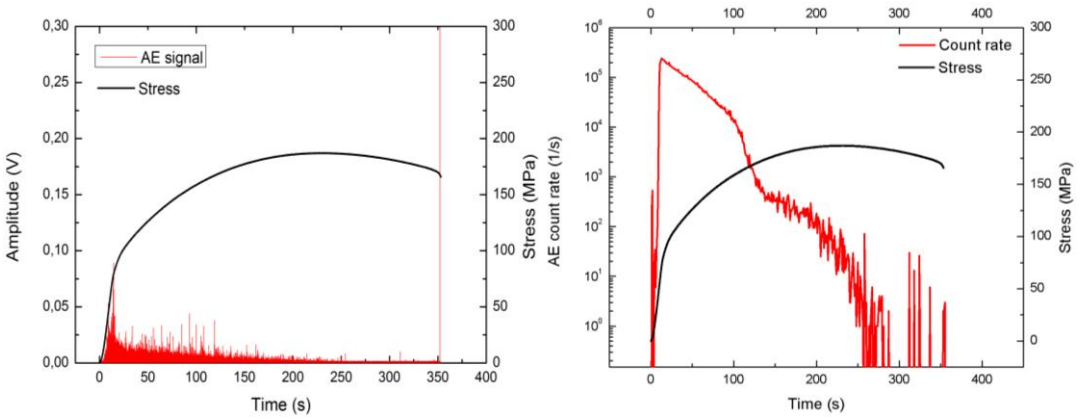

Fig. 3.15. Tensile test of MN11 alloy along the ED with concurrent AE measurement

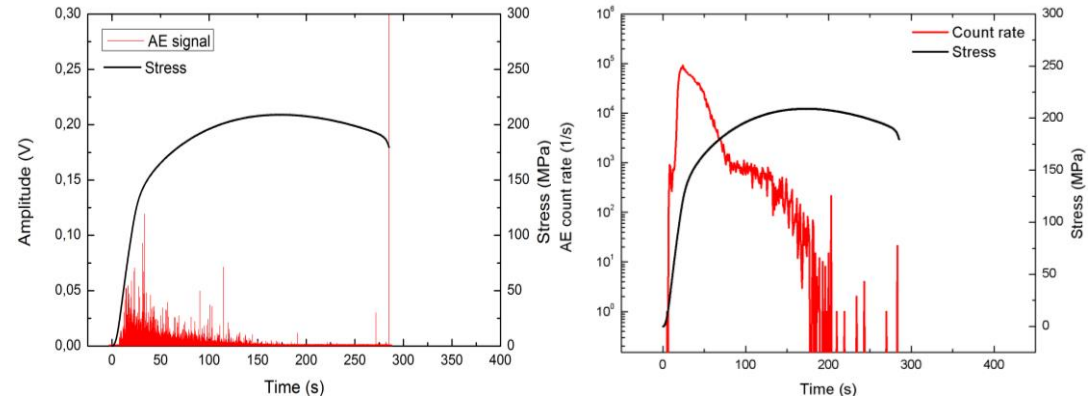

Fig. 3.16. Tensile test of MN11 alloy along the TD with concurrent AE measurement

The time dependence of the tensile stress, the AE count rate and the AE signal for the ZN11 alloy is plotted in Fig. 3.17 and 3.18, respectively. The AE response, with the high amplitude signal and the maximum of the AE count rate at the onset of plastic deformation in the ED sample, is similar to previous Mg alloy. Likewise, the following decrease in the AE count rate is more pronounced in the TD than in the ED sample. As the plastic deformation proceeds, the AE signal with relatively high amplitude can be found. The high amplitude AE signal can be correlated to the inflexion points on deformation curve.

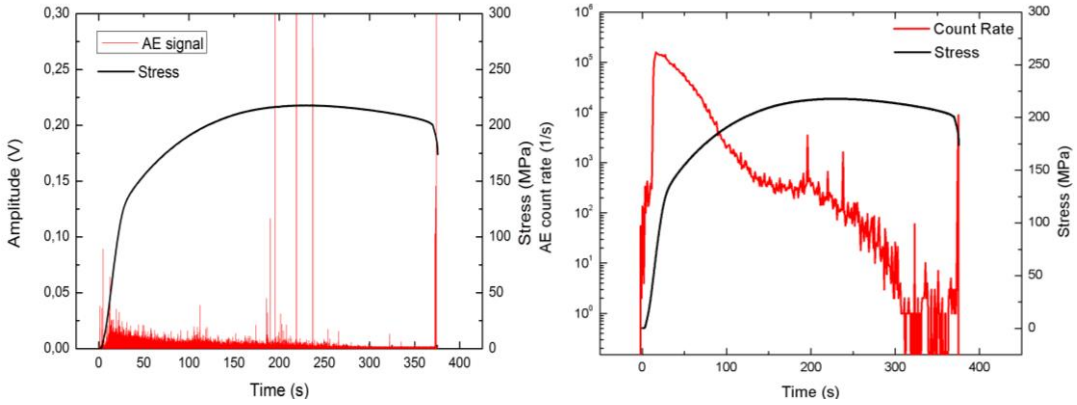

Fig. 3.17. Tensile test of ZN11 alloy along the ED with concurrent AE measurement

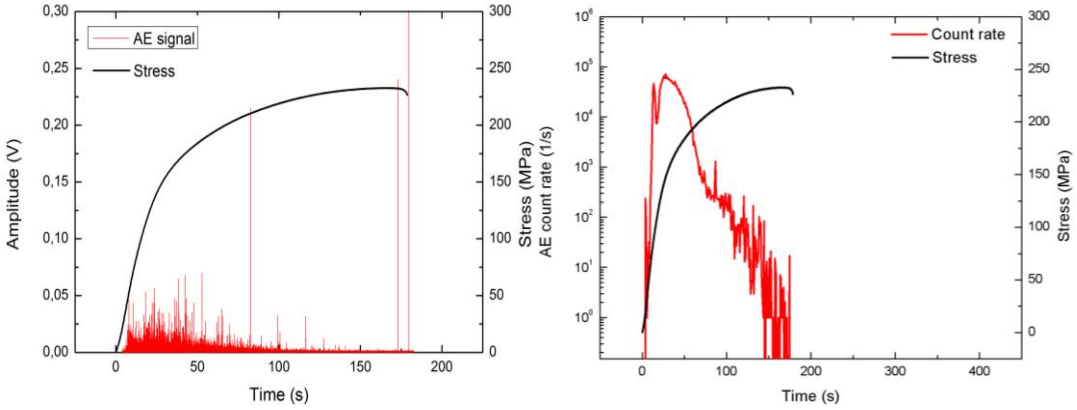

Fig. 3.8. Tensile test of ZN11 alloy along the TD with concurrent AE measurement

The tensile stress, the AE count rate and the AE signal *vs.* time curves for the ZK10 alloy are plotted in Fig. 3.19 and 3.20, respectively. At very early stage of plastic deformation, higher amplitudes of the AE signal for the tensile loading along the ED than the TD were observed. After the YS, higher amplitudes are found in the TD. The AE count rate exhibits two distinctive peaks. The first peak is correlated with the macroscopic yield point and the second one can be related to the geometrical instability (necking) in the material. More pronounced decrease in the AE count rate was found during deformation along the ED.

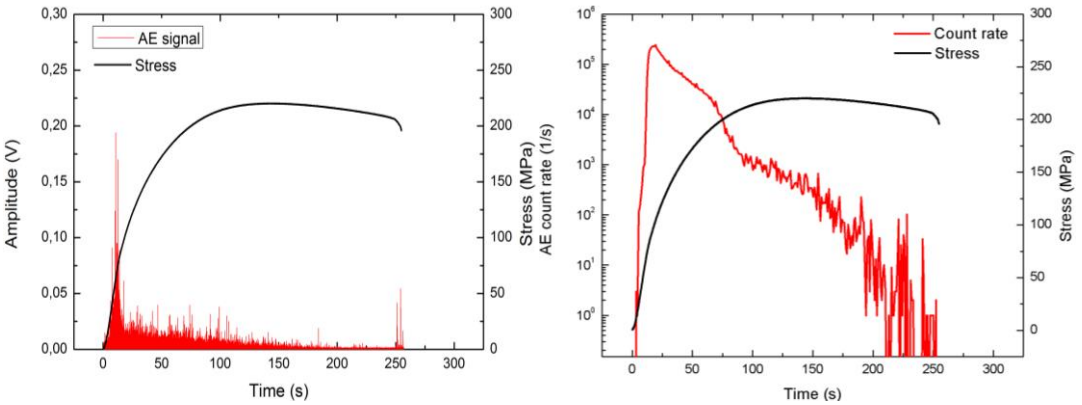

Fig. 3.19. Tensile test of ZK10 alloy along the ED with concurrent AE measurement

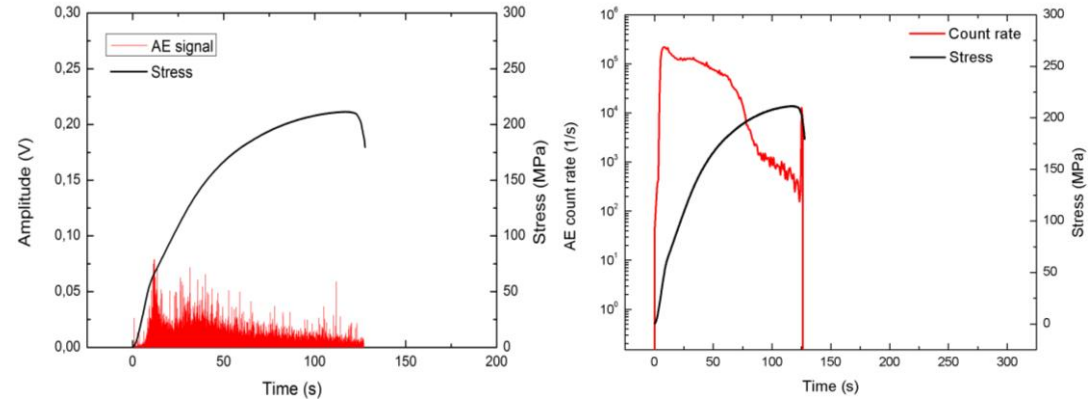

Fig. 3.20. Tensile test of ZK10 alloy along the TD with concurrent AE measurement

The time dependence of the compressive stress, the AE count rate and the AE signal for the MN11 alloy are presented in Figs. 3.21 – 3.23. In the ED and TD samples, high-amplitude AE signals at the onset of plastic deformation are detected. In the ND sample, only a low amplitude signal is measured. The maximum of the AE count rate is detected at the macroscopic yield point and the following decrease is connected with a strong work hardening on the deformation curve. The highest AE activity is detected in the TD sample and the smallest one in the ND sample. By comparison with tensile tests (Figs. 3.15, 3.16), during compression, the amplitude of the AE signal at very early stage of plastic deformation is significantly higher. On the other hand, during tensile loading the AE activity persists till the end of the test.

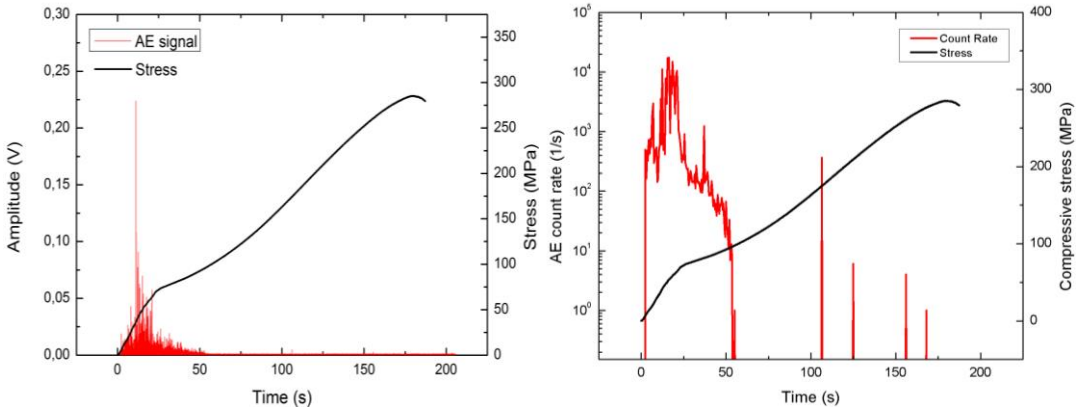

Fig. 3.21. Compression test of MN11 alloy along the ED with concurrent AE measurement

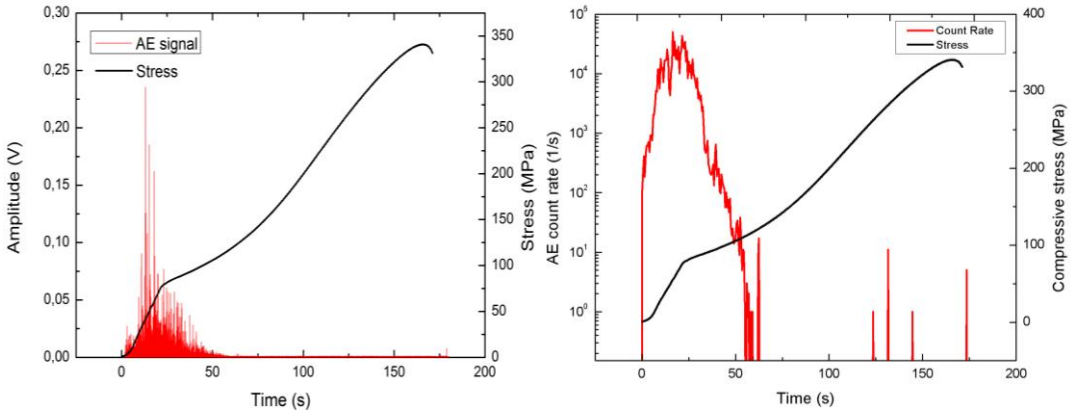

Fig. 3.22. Compression test of MN11 alloy along the TD with concurrent AE measurement

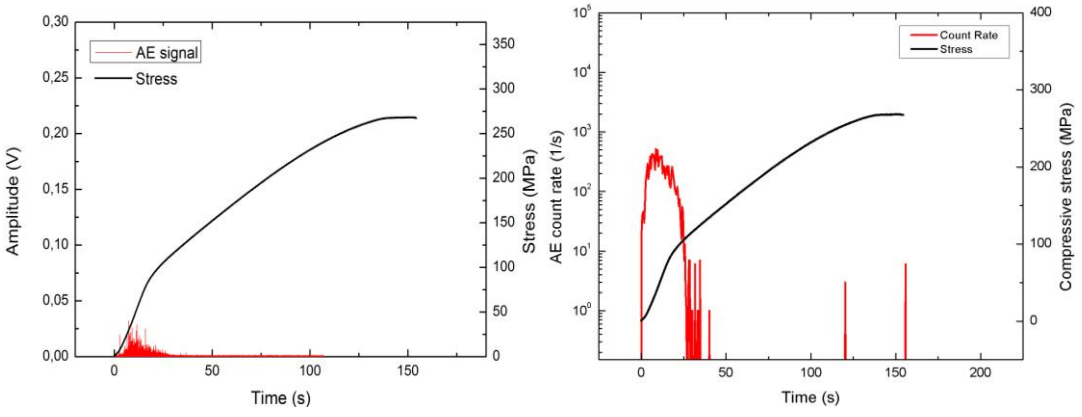

Fig. 3.23. Compression test of MN11 alloy along the ND with concurrent AE measurement

The stress, the AE count rate and the AE signal *vs.* time curves for the ZN11 alloy compressed along three directions are presented in Figs. 3.24 – 3.26. The AE activity is similar to those observed in the MN11 alloy, i.e. the AE signal vanish shortly after the YS and the AE count rate exhibits its maximum at the YS. Furthermore, the strongest AE signal is detected in the TD sample and a very low amplitude signal, near the YS, is observed in the ND sample. For the ED and TD samples, a relative strong AE activity was found at later stage of plastic deformation.

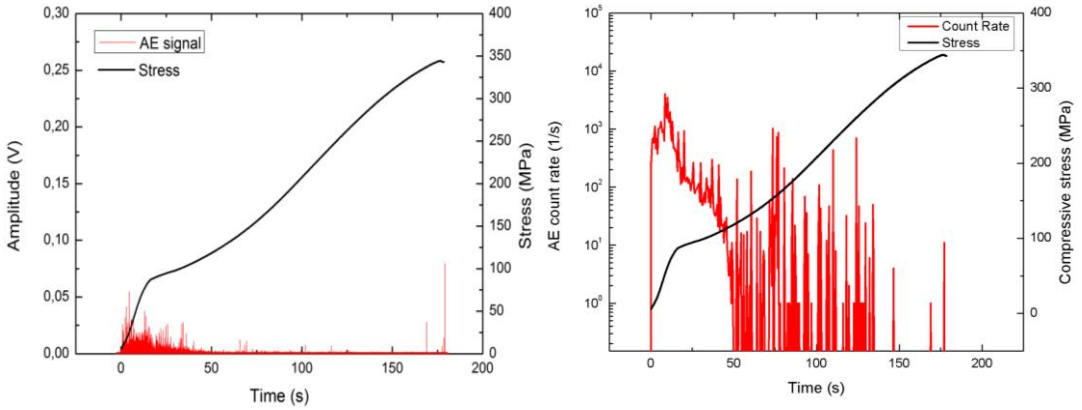

Fig. 3.24. Compression test of ZN11 alloy along the ED with concurrent AE measurement

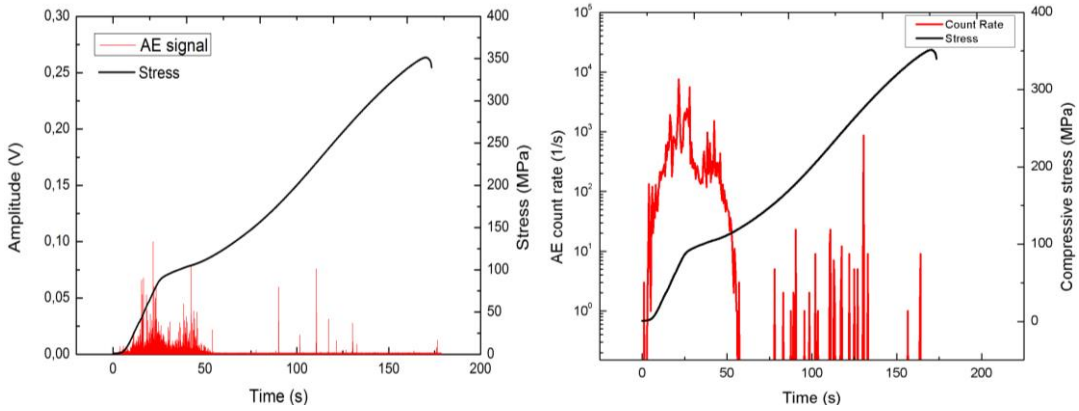

Fig. 3.25. Compression test of ZN11 alloy along the TD with concurrent AE measurement

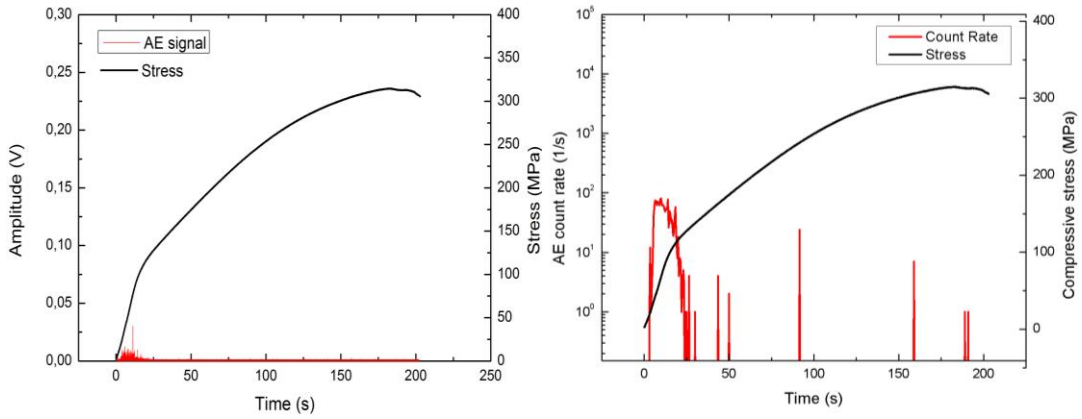

Fig. 3.26. Compression test of ZN11 alloy along the ND with concurrent AE measurement

Compressive stress, the AE count rate and the AE signal *vs.* time curves for the ZK10 alloy are presented in Figs. 3.27 – 3.29. The amplitude of the AE signal is significantly higher in the ED sample than in the TD and ND samples. The AE activity rapidly decreases to zero after the YS and some AE counts can be seen short before fracture of the sample. Higher amplitudes of AE signals are detected in compression than in tension (Figs. 3.19 and 3.21.). By comparison of all ND samples, the highest AE activity was observed in the ZK10 alloy.

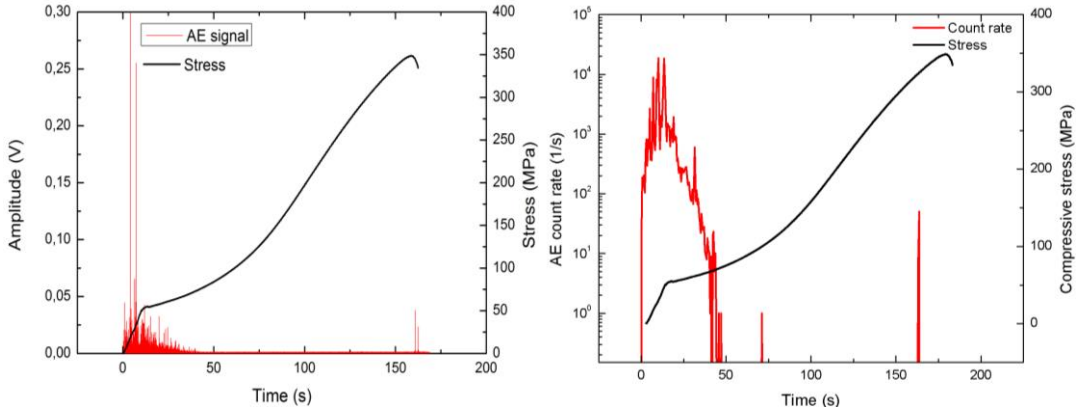

Fig. 3.27. Compression test of ZK10 alloy along the ED with concurrent AE measurement

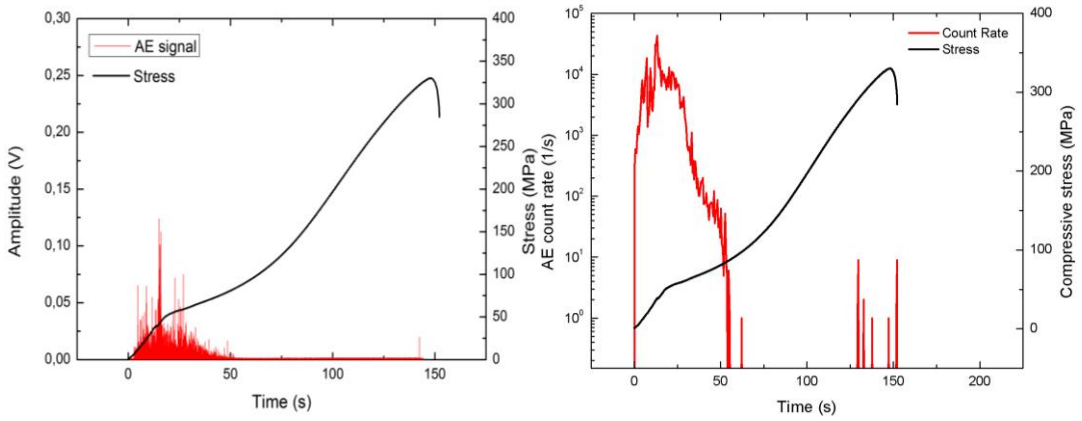

Fig. 3.28. Compression test of ZK10 alloy along the TD with concurrent AE measurement

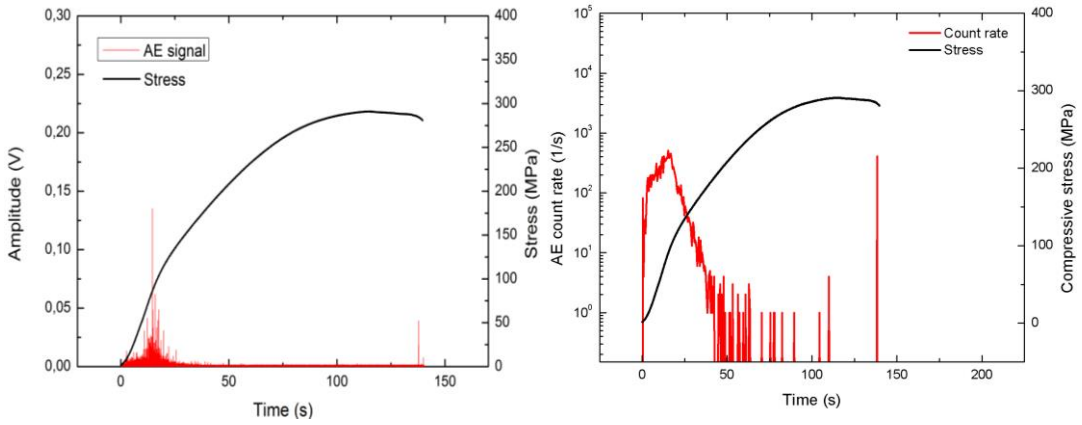

Fig. 3.29. Compression test of ZK10 alloy along the ND with concurrent AE measurement

3.4. Texture evaluation

The true stress, strain hardening rate and AE count rate *vs.* true strain curves for the ZK10 alloy compressed in the ED, TD and ND are presented in Figs. 3. 30 – 3.32. After the YS, an increase in the strain hardening rate can be seen and its maximum correlates with the inflection point on the deformation curve (for ED and TD samples). After this point, softening processes start to be active. In the ND sample, the strain hardening rate rapidly decreases till the end of the test.

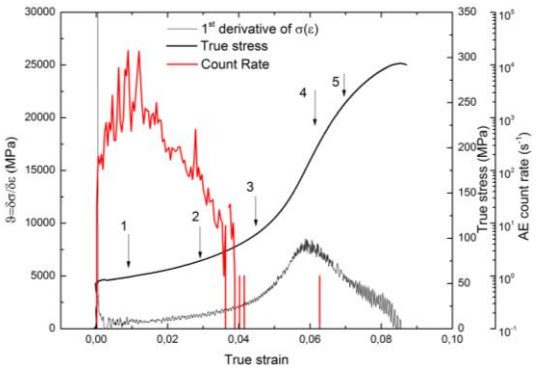

Fig. 3. 30. Stress and strain hardening rate vs. strain curves correlated with the acoustic emission count rate for ZK10 alloy compressed along the ED

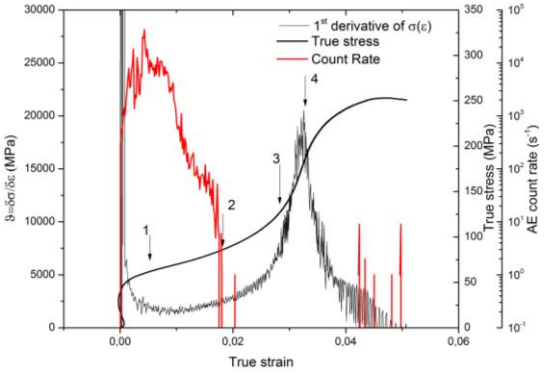

Fig. 3. 31. Stress and strain hardening rate vs. strain curves correlated with the acoustic emission count rate for ZK10 alloy compressed along the TD

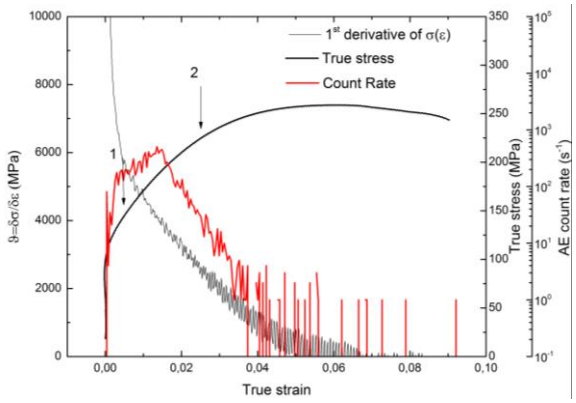

Fig. 3. 32. Stress and strain hardening rate vs. strain curves correlated with the acoustic emission count rate for ZK10 alloy compressed along the ND

Based on performed experiments on the ZK10 alloy, the samples were compressed up to specific stresses (see Figs. 3.30 – 3.32) in order to reveal the evolution of crystallographic texture during compression tests.

The results of texture measurements are shown in Figs. 3.33 – 3.35. For the ED sample deformed to the YS (Fig. 3.33, position 1), an increase in the intensity of basal pole in the (0001) pole figure, by comparing with as extruded condition, can be seen. After compression up to 75 MPa (Fig. 3.33, position 2), the angular spread of basal planes toward the TD is observed. Furthermore, two components in the (0001) pole figure towards the ED are found. As deformation proceeds (Fig. 3.33, ED,

position 3-5), the intensity of basal pole in the center of the (0001) pole figure is reduced and for the two components towards the ED rapidly increases. In other words, after compression along ED the basal planes are perpendicular to ED (Fig. 3.33, ED, position 5).

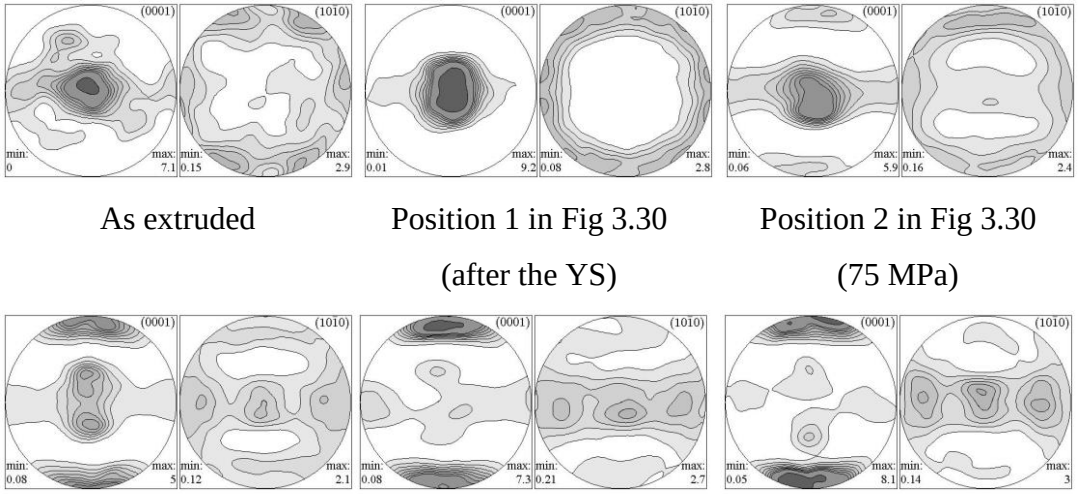

As extruded | Position 1 in Fig 3.30 (after the YS) | Position 2 in Fig 3.30 (75 MPa)

Position 3 in Fig. 3.30 (100 MPa) | Position 4 in Fig. 3.30 (200 MPa) | Position 5 in Fig 3.30 (250 MPa)

Fig. 3.33. The evolution of crystallographic texture in ZK10 alloy during compression along the ED (ED↑, TD→)

Compression of the TD sample up to the YS has a slight impact on the texture. The intensity of basal pole in the (0001) pole figure is the same and two weak components along the TD are formed (Fig. 3.34, position 1). Higher applied stresses contribute to the strengthening of both basal components along the TD (Fig. 3.34, position 2-4). Similarly to the compression along the ED sample, the intensity of the basal pole in the center of (0001) pole figure is rapidly decreasing, while the intensity of the new components toward the TD are increasing. At very late stage of plastic deformation, the basal planes are perpendicular to the TD (Fig. 3.34, position 4).

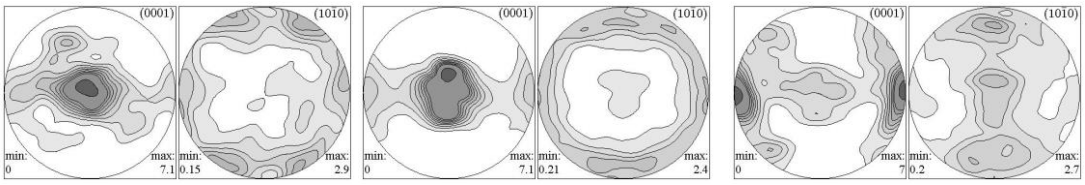

As extruded | Position 1 in Fig 3.31 (after the YS) | Position 2 in Fig 3.31 (85 MPa)

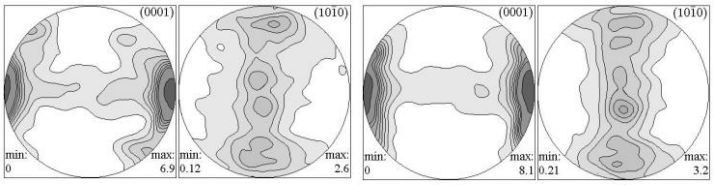

Position 3 in Fig 3.31 (130 MPa) | Position 4 in Fig 3.31 (190 MPa)

Fig. 3.34. The evolution of crystallographic texture in ZK10 alloy during compression along the TD (ED↑, TD→)

During compression of the ZK10 alloy along the ND (Fig. 3.35), the crystallographic texture is only slightly changed. The basal planes in the (0001) pole figure remain perpendicular to the ED till the end of the test and their intensity increases with increasing plastic deformation.

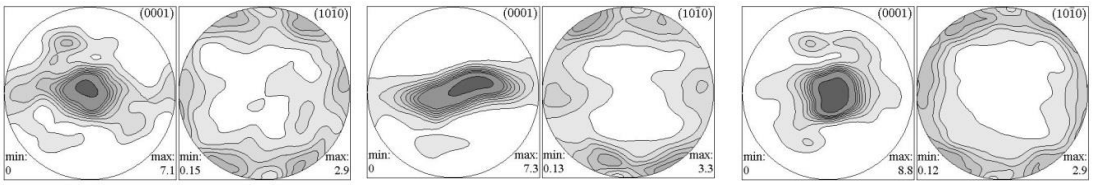

As extruded | Position 2 in Fig 3.32 (140 MPa) | Position 3 in Fig 3.32 (220 MPa)

Fig. 3.35. The evolution of crystallographic texture in ZK10 alloy during compression along the ND (ED↑, TD→)

Similarly to the deformation tests on the ZK10 alloy, the ZN11 samples were compressed up to specific stresses for a study of the crystallographic texture evolution (Figs. 3. 36, 3.37). The work hardening behavior is similar for both ZK10 and ZN11. The maximum of the strain hardening rate can be related to the inflection point on stress – strain curve.

The results of texture measurements are presented in Fig. 3. 38 and 3.39. After compression along the ED up to the YS (Fig. 3.38, position 1) no significant changes in crystallographic texture can be observed in the (0001) pole figure in comparison with the as extruded texture. With increasing stress (Fig. 3.38, position 2 and full compression) two new components of basal planes in the (0001) pole figure are observed toward the ED. After fracture, a quite intensive texture with basal planes perpendicular to the ED can be seen.

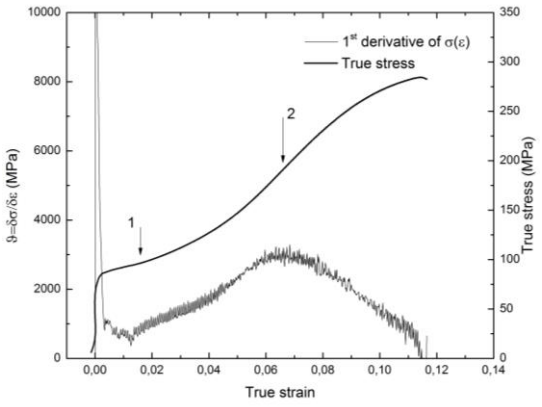

Fig. 3.36. Stress and strain hardening rate vs. strain curves for ZN11 alloy during compression along the ED

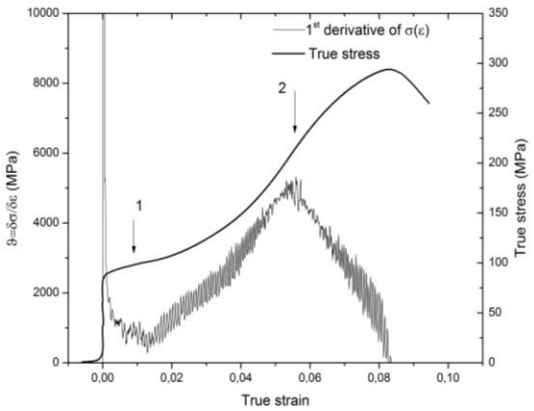

Fig. 3.37. Stress and strain hardening rate vs. strain curves for the ZN11 alloy during compression along the TD

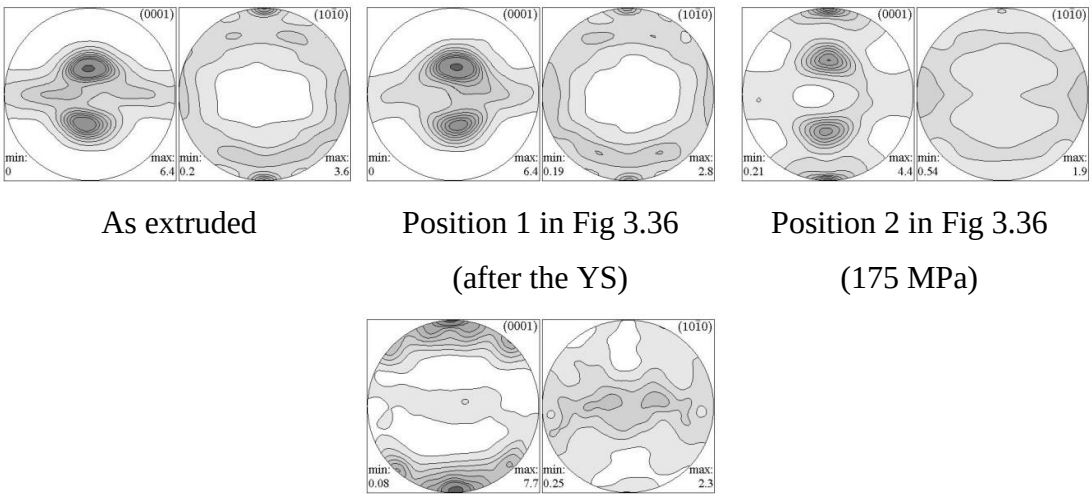

As extruded | Position 1 in Fig 3.36 (after the YS) | Position 2 in Fig 3.36 (175 MPa)

After fracture

Fig. 3.38. The evolution of crystallographic texture in ZN11 alloy during compression along the ED (ED↑, TD→)

The compression of the TD sample up to the YS results a weaker texture by comparison to as extruded condition. Moreover, spread of basal planes toward the TD is observed (Fig. 3.39, position 1). With increasing applied stress basal planes are wider broad toward the TD (Fig. 3.39, position 2 and after fracture). After compression, the basal planes are perpendicular to the TD (Fig. 3.39, after compression).

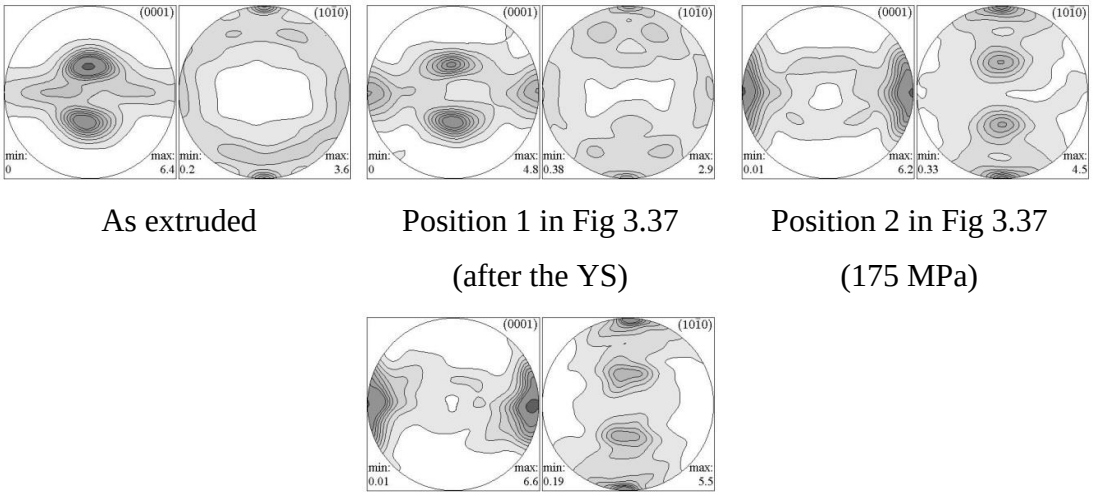

As extruded | Position 1 in Fig 3.37 (after the YS) | Position 2 in Fig 3.37 (175 MPa)

After fracture

Fig. 3.39. The evolution of crystallographic texture in ZN11 alloy during compression along the TD (ED↑, TD→)

4. Discussion

In earlier work [20] has been reported that a slow extrusion can lead to a formation of a bimodal microstructure consisting from grains elongated in the ED and small recrystallized grains. Bimodal microstructure can significantly affect the deformation behavior of Mg alloys (e.g. twinning activation [37]). It was shown in [38, 39] that an increase in the strain rate can reduce the ductility in Mg alloys with inhomogeneous microstructure. By comparing the microstructure of all three Mg alloys (Fig. 3.1 - 3.3) we can see that the microstructure of the MN11 and ZN11 alloys is homogeneous with the average grain size of 17 and 12 μm, respectively. Therefore, the extrusion speed of 3.3 mm/s seems to be appropriate for a production of MN11 and ZN11 alloys in form of rectangular profiles. It was observed in [40, 41] that zirconium (Zr) reduces the grain size in aluminum-free Mg alloys. However, the microstructure of the ZK10 alloy, in comparison with the other two Mg alloys, contains bigger grains. Thus, the microstructure after extrusion is significantly influenced not only by alloying elements, but also by the extrusion speed. According to results presented in [20], during fast extrusion, the rise of temperature can initiate static recrystallization and/or grain growth. Extrusion conditions, used in the production of the ZK10 alloy in form of rectangular profile, lead to not fully recrystallized and inhomogeneous microstructure.

In all investigated Mg alloys, crystallographic texture with basal planes (0001) nearly parallel to the ED was observed. Similar texture can be typically seen in extruded Mg alloys [20, 22, 37, 42, 43]. The texture of the MN11 and ZN11 alloys is comparable, where a slight higher intensity of basal planes was detected in the MN11 alloy. It is interesting to note that texture in extruded ZN11 is similar to texture, which was observed in rolled ZE10 sheet [42]. In the ZE10 sheet, the spread of basal planes towards the TD is responsible for changes in deformation behavior (tensile anisotropy). It was shown in [44] that an addition of rare earth elements (e.g. cerium, neodymium) leads to a weaker texture. This finding may explain the strongest texture in the rare earth elements - free ZK10 alloy, studied in this work.

From results of microhardness experiments it is clearly seen that the annealing process at 300 °C has no significant influence on the microstructure. Investigation of the texture of ZK10 alloy has shown that annealing at 300 °C as well

as at 400 °C does not affect the initial texture. The annealed microstructures exhibit only slight increase in the grain sizes compared to as received conditions. Based on above mentioned results, we can assume that the extruded Mg alloys have a stable microstructure and therefore the heat treatment is not required before mechanical testing.

The tensile deformation curves have a shape, which is typical for polycrystalline materials. The MN11 and ZN11 alloy exhibits relative strong in-plane anisotropy in tensile properties due to a distinct basal texture. Since, the pole intensity of the tilted basal planes and the tilt angle is higher in the ED than in the TD, loading in the ED is advantageous for basal 〈a〉 slip. Consequently, the YS in the ED is lower than in the TD. Similar deformation behavior can be seen in wrought Mg alloys with a strong basal texture (e.g. in [42, 45]). The absence of the YS anisotropy in ZK10 can be explained by the angular tilt of the basal planes, which are nearly symmetrically distributed along the ED and TD. Higher YS in the finer-grained MN11 and ZN11 than in the ZK10 alloy is consistent with the Hall-Petch relation [5].

With respect to the strong basal texture in extruded Mg alloys, twinning can be activated either during compressive loading in direction parallel to basal planes (ED and TD) or during tensile loading in a direction perpendicular to the basal planes (ND) [21, 46, 47]. Therefore, during tensile loading, twinning almost does not contribute to the overall deformation [48].

The S-shape of the compression curves for ED and TD samples is a typical sign of twinning activity. Activation of twins reduces the YS and is responsible for a plateau on deformation curve. Twinning causes a crystal lattice re-orientation of 86.3° around the $(10\bar{1}2)$ plane and plastic deformation is realized by a dislocation slip in the reoriented basal planes [49, 50]. Newly formed twins are obstacles for moving dislocations and therefore significantly contribute to strain hardening. Compression along the ND, i.e. compressive loading in a direction perpendicular to the basal planes, is not favorable for twinning activity and deformation curve is similar to tensile curves for ED and TD samples. Plastic deformation is firstly realized by basal slip and subsequently non-basal slip systems can be activated. This explains the highest YS, detected in the ND for all examined Mg alloys. Similarly to tensile tests, MN11 and ZN11 exhibit in-plane anisotropy also in compression due to

a strong basal texture. The tilt of the basal planes in the ED is higher than in TD, what favors twinning in the ED and results in lower YS in ED than in TD [51].

The compression-tension asymmetry at the YS is the result of the hcp lattice and a strong deformation texture, which was formed during the extrusion process. In randomly orientated polycrystalline Mg alloys, more grains are favorable orientated for extension twinning in compression than in tension. In tension, the tilt angle of the c-axis from the ideal (vertical) position for tensile twinning is 64° 53′, while in compression the tilt from the horizontal position is 45° 51′ [52-54]. The smallest YS asymmetry is found in a relatively fine-grained MN11 alloy deformed along the ED. It has been proven that a grain refinement in Mg alloys may reduce the tension-compression asymmetry at the YS due to the reduction of the influence of twinning on the total deformation [55]. On the other hand, the second smallest tension-compression asymmetry at the YS is observed in inhomogeneous ZK10 alloy deformed along the TD.

The AE count rate of the tensile and compression tests cannot be quantitatively compared due to different volumes and shapes of the samples. However, the decrease in the AE count rates after the yield point is more pronounced in compression than in tension, what reflects a much stronger effect of strain hardening. Similar behavior of AE count rates was documented in [56]. It has been shown in [57] that the grain size has an influence on the AE activity, where the AE count rate decreases with decreasing average grain size. It can be explained by a large free path for a collective motion of dislocations in large grains, while in the fine-grained microstructure higher amount of grain boundaries, which are obstacles for the dislocation motion, are present. Some studies have also shown [57, 58] the dependence of AE on the grain size distribution, preferred orientation and on the character and distribution of precipitates. All these mechanisms have an influence on the activation and distribution of dislocation avalanches and an occurrence of twins.

In tensile tests, the AE maximum at the beginning of plastic deformation is usually explained by the massive multiplication of dislocations. Therefore in MN11 and ZN11, higher AE count rate at the YS in ED than in TD sample can be related to easier activation of basal slip during deformation along the ED. In the ZK10 alloy, with respect to the symmetrical distribution of basal planes along the ED and TD (Fig. 3.3), similar AE count rate at the YS is observed for both ED and TD samples.

The following decrease in the AE count rate is caused by forest dislocations, which act as obstacles for moving dislocations. For MN11 and ZN11, more significant decrease is observed in TD than ED samples. Nevertheless, the AE activity persists till the end of the test. According to [59, 60], during tensile tests, twins can be nucleated, however, they need higher stresses and their growth is limited. Therefore, an occurrence of twins, necessary for a compatible plastic deformation, could be found at later stage of tensile loading. The highest AE count rate during tensile deformation is detected in ZK10 alloy, which has the largest grains.

During compression of extruded Mg alloys, besides basal slip, twinning is a primary activated mechanism. It is an excellent source of AE [57] and it is responsible for strong AE signals. It was documented in [61, 62] that the twin nucleation produces detectable AE signal contrary to twin growth. Therefore, a reduction of the AE activity can indicate a decrease of twinning activity (twin nucleation). Despite no AE at higher strains in the MN11 and ZK10 alloys, the dislocation glide will continuously be activated to accommodate strain in a heavily deformed material up to fracture [22]. The AE count rate in the ZN11 alloy is different from the previous two Mg alloys. Occurrence of the AE activity at later stage of plastic deformation can be atributted to nucleation of twins.

In order to study the texture evolution during compression, the deformation tests were repeated to successively greater strains along the stress-strain curve. The choice of strains (specific points on deformation curve) was based on changes of deformation behavior and the AE response. For the ZK10 alloy, 5 specific points on deformation curve in ED and 4 in TD loading were chosen. For the ZN11 alloy, two deformation tests were repeated to different strains.

At the very early stage of deformation, before the macroscopic yield point, AE activity was detected. The AE signal is caused by the microplastic deformation, which occurs in favorable oriented grains for dislocation slip before the YS. Similar AE behavior was also documented in [37, 51, 54, 63]. The massive multiplication of dislocations and a nucleation of twins at the YS produce strong AE. The texture of ZK10 sample compressed in ED up to the YS shows an increase in the intensity of basal planes in (0001) pole figure. For position 2 on stress-strain curve (Fig. 3.32), new components towards the ED in the (0001) pole figure (Fig. 3.35) occur, what indicates on the strong twinning activity during plastic deformation between the YS

and the position 2. Tensile twins can reorient the basal planes by 86.3° to original orientation [49, 50] and basal planes are perpendicular to the loading direction. Therefore, due to a massive twinning, a very high AE activity was measured. Afterwards, with increasing strain hardening, AE disappears and the intensity of the newly formed basal components in the (0001) pole figure (Fig. 3.32, pos. 3 and 4) increases. Thus, plastic deformation is manly realized by dislocation slip and growth of twins, which cannot contribute to detectable AE. After compression along the ED, the basal planes are almost completely reoriented and displayed in the (0001) pole figure as very strong components towards the ED.

As the result of the symmetrically distributed $\{10\bar{1}0\}$ prismatic planes in (10-10) pole figures (Fig. 3.32), the compression along the TD has similar effect on texture like the compression along the ED. The AE activity decreases more rapidly in the TD than in ED, what can be explained by higher strain hardening rate. After compression along the TD, the basal planes in the (0001) pole figure are perpendicular to the loading direction.

In compression along the ND, the texture is not favorable for the twinning, because the c-axis is parallel to the loading direction. Therefore, only a slight increase in the intensity of basal planes during plastic deformation was observed. Despite of that, a relatively high AE activity is measured in the ZK10 alloy as a result of the collective dislocation motion. The results are consistent with the idea that compression along the ND is similar to tensile loading along the ED and TD. Similar results were observed for the ZN11 alloy.

The strain hardening rate depends on the loading direction. It was reported in [64, 65] that the extension twinning induces the hardening rate regime. Oppedal et al. [66] connected this regime to the Hall-Petch effect and attributed it to two different mechanisms: to texture hardening and dislocation transmutation. By comparing the final textures after the compression along the ED, TD and ND, it is clearly seen that in all cases the c-axis is parallel to the loading direction. On the other hand, the corresponding hardening behavior varies with the deformation direction. Based on [67] this variety comes from the effect of dislocation transmutation.

In the present work, AE streaming was used. Discriminating between dislocation slip and deformation twinning in the AE signal for Mg alloys is not straightforward because both mechanisms operate simultaneously; therefore the AE

stream contains contributions from both mechanisms [68]. Nevertheless, these two sources induce AE with different characteristic features. The biggest differences between these two mechanisms are commonly associated with both the shape of AE waveforms and the amplitude and power of the AE signals (low amplitude/low power AE for dislocation slip and to high amplitude/high power AE for twinning) [59, 70].

The features observed for the AE count rate, i.e. dependence on the volume of the sample, temperature, grain size distribution, etc. are also valid for the AE signal behavior. In the most presented cases the results of the AE count rate and AE signal are similar. The maximum of the amplitude of the AE signal is observed before the YS, which is related to the microplasticity of the Mg alloys (occurrence of basal slip and twinning). In tensile tests after the YS, a subsequent decrease in the AE signal is seen, however AE persists up to fracture. In ZN11, the high-amplitude signals around the inflection point could be associated with cracking in the material.

The difference between the MN11 and ZN11 alloys compression tests (Figs. 3.21 – 3.26) can be explained by the higher initial dislocation density in the ZN11 alloy. Generally, increasing dislocation density reduces the mean distance and the free path for moving dislocation and results in a decrease of the AE activity [71, 72]. Therefore in ZN11, the breakaway process of dislocations produces a high amplitude signal with a relative low AE count rate in comparison to MN11. Similar results were observed on Al-Si-Mg-Mn alloy [73], where with increasing annealing time the dislocation density decreases and following deformation loading led to a detection of the AE signals consisting from lower amplitudes.

Due to different volumes and shapes of the samples, the AE signals, observed during tensile and compression tests, cannot be directly compared. The AE signal detected in compression along ED and TD has 4-5 times higher amplitude than that detected for ND sample. As written above, in the ND, twinning is not preferable, and so the low amplitude AE signal can be ascribed to collective dislocation motion. On other hand, during compression along ED and TD, nucleation of twins can produce high amplitude AE signals.

5. Conclusions

The extruded profiles of MN11 and ZN11 alloys exhibit fine-grained and homogeneous microstructure after extrusion at 350 °C with an extrusion speed of 3.3 mm/s. In the ZK10 alloy, extrusion at 250 °C with an extrusion speed of 10 mm/s is responsible for an inhomogeneous microstructure.

As a result of extrusion, the basal planes are parallel to ED with c-axis parallel to ND. In the MN11 and ZN11 alloys, the basal planes are tilted into the ED and form two maxima in basal pole figure. In the ZK10 alloy the basal planes are symmetrically distributed around the center of the (0001) pole figure. The ZK10 alloy has the strongest texture.

We can assume that investegated alloys have stable microstructure, because after annealing at 300 °C resp. 400 °C their texture did not change and only slight differences in microshardness values and in microstructure were observed.

The MN11 and ZN11 alloys exhibit strong in-plane anisotropy as the result of their texture. The basal planes tilted to the ED are responsible for lower stresses (YS, UTS, UCS) in tensile loading along the ED (easier activation of basal slip) and in compression along the ED (easier twinning activation). The ZK10 with its symmetrical texture has similar tensile curves for ED and TD samples.

Compression along the ND, i.e. compressive loading in a direction perpendicular to the basal planes, is not favorable for twinning and deformation curve is similar to tensile curves for ED and TD samples.

During tensile loading of all Mg alloys, a relative high AE activity persists till the end of the test, while in compression only in the ZN11 alloy a significant AE activity after the yield point is observed. At later stages of tensile deformation, twin nucleations can ocurs.

AE signal is measured before the macroscopic yield point as the result of microplasticity (basal slip and/or twinning).

The texture evolution was investigated during compression. Twinning occurs around the yield point (in ED and TD samples), increases the strain hardening rate and consequently decreases the AE activity. At the end of the compression (along all directions) the c-axis gets parallel to the loading direction. During compression along ND no significant texture changes can be observed.

Options for further research

Based on the present work, the ZN11 seems to have the best characteristics. It has homogeneous fine-grained microstructure, with relatively low texture intensity. As the result of its texture, low anisotropy is observed in this alloy with acceptable YS asymmetry.

The twin volume fraction during compressive loading should be investigated by electron backscattered diffraction (EBSD) measurement. Together with X-ray diffraction analysis, important information about twinning during compression can be achieved.

In order to study twinning-detwinning behavior of extruded profiles, low-cyclic tests (compression-tension) could be measured with concurrent AE activity.

The raw AE signal can be subjected to further processing using of AE parameters in order to distinguish dislocation slip from mechanical twinning. Characterization and better understanding of twinning in Mg alloys contributes to achievement such an improvement of their mechanical properties.

Further statistical processing of the obtained AE parameters (i.e. the amplitude or the energy of emission events) can be used for a study of dislocation dynamic during plastic deformation.

Bibliography

[1] http://kdf.mff.cuni.cz/~koudelkova/U3V/Drozd_horcik.pdf *(status to the day 06/05/2015).*

[2] Avedesian, M. M. and H. Baker: *Magnesium and Magnesium Alloys (ASM Specialty Handbook). Edtion ed.: ASM International, (1999). ISBN 0-87170-657-1.*

[3] J. Kaiser: *Dr. – Ing. Dissertation: Untersuchung über das Auftreten von Geräuschen beim Zugversuch, TU München (1950).*

[4] J. Lubliner, *Plasticity theory, Dover (2008).*

[5] P. Kratochvíl, P. Lukáč, B. Sprušil: *Úvod do fyziky kovů I., Praha (1984).*

[6] G. Ananthakrishna: *Current theoretical approaches to collective behavior of dislocations, Phys. Rep., 440 (2007), 113–259.*

[7] R. von Mises: *Mechanik der plastischen Formaenderung von Kristallen, Z. Angew. Math. Mech., 6 (1928), 85.*

[8] K. Máthis: *Doktori értekezés: Deformációs mechanizmusok magnézium alapú könnyűfém ötvözetekben, ELTE, Általános Fizika Tanszék (2004).*

[9] R. L. Bell, R. W. Cahn: *The Dynamics of Twinning and the Interrelation of Slip and Twinning in Zinc Crystals, Proc. Rpy. Soc. 239 (1957), 494.*

[10] M.R. Barnett: *Twinning and the ductility of magnesium alloys. Part I: Tension twins, Mater. Sci. Eng. A, Structural Materials, 464 (1–2) (2007), 1–7.*

[11] https://wwwf.imperial.ac.uk/earthscienceandengineering/rocklibrary/learntwinning1.php *(status to the day 06/05/2015).*

[12] K. Máthis, P. Beran, J. Čapek, P. Lukáš: *In-situ neutron diffraction and acoustic emission investigation of twinning activity in magnesium, Journal of Physics: Conference Series 340 (2012), 012096.*

[13] P. Dobroň: *Doktorská dizertačná práca: Štúdium mechanických a fyzikálnych vlastností nových, konštrukčných materiálov na báze horčíka metódou akustickej emisie, MFF UK (2007).*

[14] http://130.149.194.171/lib/html/en/strpr_hydro.php *(status to the day 06/05/2015).*

[15] http://130.149.194.171/lib/html/en/strpr_indir.php *(status to the day 06/05/2015).*

[16] O. Duygulu, S. R. Agnew: *The effect of temperature and strain rate on the tensile properties of textured magnesium alloy AZ31B sheet, in: H. Kaplan (Ed.), Magnesium Technology 2003 TMS, San Diego, CA, USA (2003), 237.*

[17] C. J. Bettles, C. J. Gibson: *Current wrought magnesium alloys strengths and weaknesses, JOM 57 (5) (2005), 46.*

[18] K. Petruželka, J. Hrubý: Strojírenské tváření I, *VŠB – Technická univerzita Ostrava (2001), 152.*

[19] A. Jain, S.R. Agnew: *Modeling the temperature dependent effect of twinning on the behavior of magnesium alloy AZ31B sheet, Mater. Sci. Eng. A, Structural Materials, 462 (1–2) (2007), 29.*

[20] J. Bohlen, S. B. Yi, D. Letzig, K. U. Kainer: *Effect of rare earths elements on the microstructure and texture development in magnesium-manganese alloys during extrusion, Mater. Sci. Eng. A, 527 (2010), 7092–7098.*

[21] D.L. Yin, J.T. Wang, J.Q. Liu, X. Zhao: *On tension–compression yield asymmetry in an extruded Mg–3Al–1Zn alloy, J Alloys Compd, 478 (2009), 789–795.*

[22] K. Illkova, P. Dobroň, F. Chmelík, K. U. Kainer, J. Balík, S. Yi, D. Letzig, J. Bohlen: *Effect of aluminium and calcium on the microstructure, texture, plastic deformation and related acoustic emission of extruded magnesium-manganese alloys, Journal of Alloys and Compounds, Volume 617 (2014), 253-264.*

[23] F.S. Pan, M.B. Yang, J. Shen, L. Wu: *Effects of miner Zr and Sr on as-cast microstructure and mechanical properties of Mg-3Ce-1.2Mn-0.9Sc (wt.%) magnesium alloy, Mater. Sci. Eng. A, 528 (2011), 4292–4299.*

[24] G. Ben-Hamu, D. Eliezer, K.S. Shin, S. Cohen: *The relation between microstructure and corrosion behavior of Mg-Y-RE-Zr alloys, J. Alloys Compd., 431 (2007), 269–276.*

[25] L. Nascimento, S. Yi, J. Bohlen, L. Fuskova, D. Letzig, K. U. Kainer: *High cycle fatigue behaviour of magnesium alloys, Procedia Engineering, 2 (2010), 743-750.*

[26] V. Herrera-Solaz, P. Hidalgo-Manrique, M. T. Pérez-Prado, D. Letzig, J. Llorca, J. Segurado: *Effect of rare earth additions on the critical resolved shear stresses of magnesium alloys, Materials Letters, 128 (2014), 199-203.*

[27] Akustická emise – Metodické pokyny, *Smernica celoštátneho defektoskopického strediska, Brno* (*1987).*

[28] M. Huang, L. Jiang, P. K. Liaw, C.R. Brooks, R. Seeley, D.L. Klarstrom: *Using acoustic emission in fatigue and fracture materials research, JOM-e 50 (1998).*

[29] *Zkoušení materiálů a výrobků metodou akustické emise – Názvosloví*, Smernica celoštátného defektoskopického strediska (*1987).*

[30] C. H. Heiple, S. H. Carpenter, *Acoustic emission from Dislocation Motion, J. R. Matthews (Ed.), Acoustic Emission, Gordon and Breach Science Publisher, New York (1983), 15.*

[31] J. Baram, M. Rosen: *On the nature of the thermoelastic martensitic phase transformation in Au-47.5 at.% Cd determined by acoustic emission, Acta Metall. 30 (1982), 655-662.*

[32] E. Email, I. Grabec: *Quantitative analysis of acoustic emission during martensitic transformation of the β-CuZnAl alloy, J.Phys. D 12 (1986), 605.*

[33] J. Xu, E.-H. Han, X. Wu: *Acoustic emission response of 304 stainless steel during constant load test in high temperature aqueous environment, Corros. Sci. 63 (2012), 91.*

[34] B. Legros, P.-X. Thivel, Y. Bultel, M. Boinet, R.P. Nogueira: *Acoustic emission: Towards a real-time diagnosis technique for Proton Exchange Membrane Fuel Cell operation, J. Power Sources 195/24 (2010), 8124.*

[35] Acoustic Emission Standard Terminology ASTM E1316-05

[36] http://www.dakel.cz/index.php?pg=prod/sens/midi *(status to the day 06/05/2015).*

[37] P. Dobroň, F. Chmelík, S. Yi, K. Parfenenko, D. Letzig, J. Bohlen: *Grain size effects on deformation twinning in an extruded magnesium alloy tested in compression, Scripta Mater. 65 (2011) 424-427.*

[38] Z.Y. Nan, S. Ishihara, T. Goshima: *Corrosion fatigue behavior of extruded magnesium alloy AZ31 in sodium chloride solution, Int J Fatigue, 30 (2008), 1181–1188.*

[39] L. Jiang, J.J. Jonas, A.A. Luo, A.K. Sachdev, S. Godet: *Twinning-induced softening in polycrystalline AM30 Mg alloy at moderate temperatures, Scripta Mater, 54 (5) (2006), 771–775.*

[40] D. H. StJohn, M. Qian, M. A. Easton, P. Cao, Z. Hildebrand: *Grain Refinement of Magnesium Alloys, Metall. Mater. Trans A 36 (2005), 1669.*

[41] M. Qian, A. Das: *Grain refinement of magnesium alloys by zirconium: Formation of equiaxed grains, Scripta Mater. 54 (2006), 881.*

[42] S.B. Yi, J. Bohlen, Frank Heinemann, D. Letzig: *Mechanical anisotropy and deep drawing behaviour of AZ31 and ZE10 magnesium alloy sheets, Acta Mater. 58 (2010), 592-605.*

[43] J. Victoria-Hernandez, S. Yi, D. Letzig, D. Hernandez-Silva, J. Bolen: *Microstructure and texture development in hydrostatically extruded Mg-Al-Zn alloys during tensile testing at intermediate temperatures, Acta Mater. 61 (2013), 2179-2193.*

[44] J. Bohlen, M. R. Nürnberg, J. W. Senn, S. Letzig, S. R. Agnew: *The texture and anisotropy of magnesium-zinc-rare earth alloy sheets, Acta Mater. 55 (2007), 2101-2112.*

[45] F. Kaiser, J. Bohlen, D. Letzig, A. Styczynski, Ch. Hartig, K.U. Kainer: *Anisotropic properties of magnesium sheet AZ31, Mater Sci Forum, 419–422 (2003), 315.*

[46] W. F. Hosford: *The Mechanics of Crystals and Textured Polycrystals, Oxford University Press, Oxford (1993).*

[47] T.J. Luo, Y.S. Yang, W.H. Tong, Q.Q. Duan, X.G. Dong: *Fatigue deformation characteristic of as-extruded AM30 magnesium alloy, Mater Des, 31 (2010), 1617–1621.*

[48] I. J. Polmear: *Light Alloys, Melbourne (2006).*

[49] F. A. Mirza, D. L. Chen, D. J. Li, X. Q. Zeng: *Low cycle fatigue of a rare-earth containing extruded magnesium alloy, Mater. Sci. Eng. A 575 (2013), 65-73.*

[50] D. Sarker, D. L. Chen: *Dependence of compressive deformation on pre-strain and loading direction in an extruded magnesium alloy: Texture, twinning and de-twinning, Mater. Sci. Eng. A 596 (2014), 134-144.*

[51] P. Dobroň, F. Chmelík, K. Parfenenko, D. Letzig, J. Bohlen: *On the Effect of the Extrusion Speed on Microstructure and Plastic Deformation of ZE10 and ZEK100 Magnesium Alloys - an Acoustic Emission Study, Acta Phys. Pol. A 122/3 (2012), 593-596.*

[52] S.R. Agnew, M.H. Yoo, C.N. Tome*: Application of texture simulation to understanding mechanical behavior of Mg and solid solution alloys containing Li or Y, Acta Mater., 49 (2001), 4277–4289.*

[53] G.E. Mann, T. Sumitomo, C.H. Caceres, J.R. Griffiths: *Reversible plastic strain during cyclic loading–unloading of Mg and Mg–Zn alloys, Mater. Sci. Eng. A-Struct., 456 (2007), 138–146.*

[54] J. Čapek, K. Máthis, B. Clausen, J. Stráská, P. Beran, P. Lukáš: *Study of the loading mode dependence of the twinning in random textured cast magnesium by acoustic emission and neutron diffraction methods, Mater. Sci. Eng. A 602 (2014), 25-32.*

[55] J. Jain, W. J. Poole, C. W. Sinclair, M. A. Gharghouri: *Reducing the tension–compression yield asymmetry in a Mg–8Al–0.5Zn alloy via precipitation, Scripta Mater. 62 (2010), 301.*

[56] E. M. García, P. Dobroň, J. Bohlen, D. Letzig, F. Chmelík, P. Lukáč, K.U. Kainer: *Deformation mechanisms in an AZ31 cast magnesium alloy as investigated by the acoustic emission technique, Mater. Sci. Eng. A 462 (2007), 297-301.*

[57] C. R. Heiple, S. H. Carpenter: *Acoustic Emission Produced by Deformation of Metals and Alloys – A Review: Part I, J. Acoust. Emission 6 (1987), 177.*

[58] J. Bohlen, F. Chmelík, P. Dobroň, D. Letzig, P. Lukáč, K.U. Kainer*: Acoustic emission during tensile testing of magnesium AZ alloys, J. Alloys Comp. 378 (2004), 214 – 219.*

[59] H. Yoshinaga, T. Obara, S. Morozumi: *Twinning deformation in magnesium compressed along the C-axis, Mater. Sci. Eng. A 12 (1973), 255-264.*

[60] K. Máthis, J. Čapek, Z. Zdraždilová, Z. Trojanová: *Investigation of tension-compression asymmetry of magnesium by use of the acoustic emission technique, Mater. Sci. Eng. A 528 (2011), 5904-5907.*

[61] C. R. Heiple, S. H. Carpenter: *Acoustic Emission Produced by Deformationof Metals and Alloys – A Review: Part II, J. Acoust. Emission 6 (1987), 215.*

[62] J.P. Toronchuk: *Acoustic emission during twinning of zinc single crystals, Mater.Eval*, 35 (*1977), 51*-53.

[63] A. Vinogradov, D. Orlov, A. Danyuk, Y. Estrin: *Effect of grain size on the mechanisms of plastic deformation in wrought Mg-Zn-Zr alloy revealed by acoustic emission technique, Acta Mater. 61 (2013), 20144-2056.*

[64] X.Y. Lou, M. Li, R.K. Boger, S.R. Agnew, R.H. Wagoner: *Hardening evolution of AZ31B Mg sheet, Int. J. Plast., 23 (2007), 44–86.*

[65] L. Jiang, J.J. Jonas, A.A. Luo, A.K. Sachdev, S. Godet: *Influence of {10-12} extension twinning on the flow behavior of AZ31 Mg alloy, Mater. Sci. Eng. A, 445–446 (2007), 302–309.*

[66] A.L. Oppedal, H. El-Kadiri, C.N. Tomé, G.C. Kaschner, S.C. Vogel, J.C. Baird: *Effect of dislocation transmutation on modeling hardening mechanisms by twinning in magnesium, Int. J. Plast., 30–31 (2012), 41–61*.

[67] L. Zhang, C.-G. Liu, H.-Y. Wang, X.-L. Nan, W.X. Xiao, Q.-C. Jiang: *Twinning and mechanical behavior of an extruded Mg-6Al-3Sn alloy with a dual basal texture, Mater. Sci. Eng. A, 578 (2013), 14-17.*

[68] A. Vinogradov, D. Orlov, A. Danyuk, Y. Estrin: *Deformation mechanisms underlying tension–compression asymmetry in magnesium alloy ZK60 revealed by acoustic emission monitoring, Mater. Sci. Eng. A 621 (2015), 243-251.*

[69] E. Pomponi, A. Vinogradov, European Working Group on Acoustic Emission Annual Meeting (EWGAE-2012), NDT.net Granada, Spain, 2012.

[70] E. Pomponi, A. Vinogradov: *A real-time approach to acoustic emission clustering, Mechanical Systems and Signal Processing 40 (2013), 791–804.*

[71] C.R. Heiple, S.H. Carpenter: *Acoustic emission produced by deformation of metals and alloys- A Review: Part I, J.Acoustic Emission 6 (1987), 177-204.*

[72] K. Máthis, F. Chmelík: *Exploring Plastic Deformation of Metallic Materials by the Acoustic Emission Technique, in: W. Sikorski (Ed.), Acoustic Emission, InTech, Rijeka (2012), 23–48.*

[73] O. Molnárová: Diplomová práce; *Studium nestabilní plastické deformace metodou akustické emise, MFF UK (2014).*

List of figures

List of Abbreviations

AE ..... acoustic emission

Al..... aluminum

CRSS..... critical resolved shear stress

ED ..... extrusion direction

EDAX..... energy dispersive X-ray analysis

hcp..... hexagonal close packed

Mg ..... magnesium

Mn ..... manganese

ND..... normal direction

Nd..... neodymium

RE..... rare earth elements

RT..... room temperature

TD ..... transversal direction

U_r..... reference voltage

UCS..... ultimate compression strength

UTS ..... ultimate tensile strength

YS..... yield strength

Zn ..... zinc

Zr..... zirconium

σ_m..... ultimate strength